University of Augsburg
Faculty of Applied Computer Science
Institute of Geography

Climate and Environmental Sciences

Master thesis

Landscape development and organic matter characteristics of thermokarst lake deposits in Yakutia - Siberia

Name: Julia Wiedmann
Student number: 1507724
Email address: julia.wiedmann@student.uni-augsburg.de

First evaluator: Prof. Dr. Karl-Friedrich Wetzel
Second evaluator: Prof. Dr. Peter Fiener
First supervisor: Dr. Jens Strauss
Second supervisor: Loeka L. Jongejans

Date of submission: 29.11.2019

Contents

Table of Figures

List of tables

Abbreviations and nomenclature

°C	degree Celsius
%	percent
‰	per mille
AWI	Alfred Wegener Institute
BD	bulk density
BP	before present
BS	below surface
cm	centimeter
CO_2	carbon dioxide
DOC	dissolved organic carbon
HCL	hydrochloride acid
IPCC	Intergovernmental Panel on Climate Change
kHz	kilohertz
km^2	squared kilometer
m	meter
ml	milliliter
MS	mass specific magnetic susceptibility
nA	nano Ampere
OC	organic carbon
OM	organic matter
pH	potential of hydrogen
RPM	revolutions per minute
TC	total carbon
TIC	total inorganic carbon
TN	total nitrogen
TOC	total organic carbon
vol%	volume percentage
VPDB	Vienna Pee Dee Belemnite
wt%	weight percentage
$\delta^{13}C$	isotopic ratio between stable carbon isotopes ^{13}C and ^{12}C
$\delta^{2}H$	isotopic ratio between water isotopes ^{1}H and ^{2}H
$\delta^{18}O$	isotopic ratio between oxygen isotopes ^{18}O and ^{16}O
µm	micrometer
κ	volume susceptibility
ρ_s	mineral density
φ	soil porosity

Abstract

With ongoing climate warming, Arctic permafrost undergoes fast degradation, resulting in the deepening of the seasonally unfrozen surface and deep permafrost thaw. As permafrost landscapes store huge amounts of carbon, they are becoming a source of greenhouse gases in the course of remobilization of former freeze-locked organic carbon. Large regions of the Arctic are covered by ice-rich silt deposits with huge ice wedges, known as Yedoma. Due to their high ice content, these deposits are explicitly vulnerable to changing environmental conditions. One form of permafrost degradation is the formation of thermokarst lakes. These waterbodies play an important role regarding the thermal energy balance in the ground. Understanding the development of permafrost landscapes and the processes which cause their degradation is essential for the estimation of future changes of the permafrost-carbon feedback.

The aim of this study was the reconstruction of the development of a thermokarst affected late Quaternary landscape, by analyzing the deposits' sedimentology to understand past depositional processes. Furthermore, I analysed the organic matter characteristics to identify the vulnerability of the organic carbon.
Two sediment cores below two thermokarst lakes in the Lena Aldan interfluve region in Central Yakutia were investigated. One core originates from a Yedoma site (YUK15-YU-L15), where sediments accumulated during the late Pleistocene. The other core was retrieved from the bottom of an Alas lake (YUK15-YU-L7), consisting of diagenetically and thermal altered Yedoma deposits. Underneath both lakes, a talik (unfrozen ground or thaw bulb) was present. The talik was about 12 m deep for YUK15-YU-L15 and exceeded the core depth of YUK15-YU-L7. The fieldwork was conducted in March 2015 during a joined German-Russian expedition. The two cores were analysed for hydrochemical, biogeochemical and sedimentological parameters.

The grain size distribution shows that the lake deposits of both cores were mainly accumulated by fluvial sedimentation processes. The very low organic carbon content in the deposits stand in contrast to other investigated Yedoma study sites. Reasons for the lack of carbon can be deep-thawing processes and related organic matter decomposition in the existing talik or the input of organic-poor sediments in the past. Water isotopes from pore water show a permanently frozen state for the lower part of the Yedoma lake core, thereby ruling out strong organic matter decomposition. For the Alas lake core, stable water isotopes reflect more recent precipitation values, resulting from rain and lake water infiltration in the unfrozen ground. An assumption is that the Alas lake deposits had characteristics similar to the Yedoma lake deposits before permafrost degradation. This can help to estimate future developing stages of the study site.
These findings indicate that Yedoma deposits are very heterogeneous on a global scale. The high water and ice content make these deposits vulnerable to fast permafrost degradation and ground subsidence. With the current warming scenarios, thermokarst activity will probably stay on a high level and an increase of thermokarst lake formation is likely in Central Yakutia.

1. Introduction

In the following chapter, the importance of permafrost landscapes in the Arctic regions for the global climate development is depicted. Furthermore, the aim and objectives for my master thesis are formulated.

1.1 Scientific relevance and background

Human impact on a changing Earth's climate is evident and greenhouse gas emissions are the highest in human history (IPCC, 2014). The resulting effects of global warming include self-enforcing processes like decreasing sea ice and thawing permafrost. The warming is also causing higher evaporation rates, which lead to an increasing amount of climate active water vapor in the atmosphere.

Climate models show that the increase of the global average surface temperature is expected to be in the range between 1.5 and 2.0°C at the end of the 21st century (IPCC, 2014). The global mean surface temperature has increased significantly over the past century, at a rate of 0.12°C per decade since the mid-twentieth century (Huang et al., 2017). The Arctic and Antarctic regions are even more affected by a changing and warming climate and for several decades, surface air temperatures in the Arctic have warmed approximately twice the global rate (Solomon et al., 2007). The estimated global surface temperature increase modeled by NASA (GISS surface Temperature Analysis) reaches values up to 5.8°C in the Arctic and Antarctic regions, compared to the 1951-1980 interval (Figure 1).

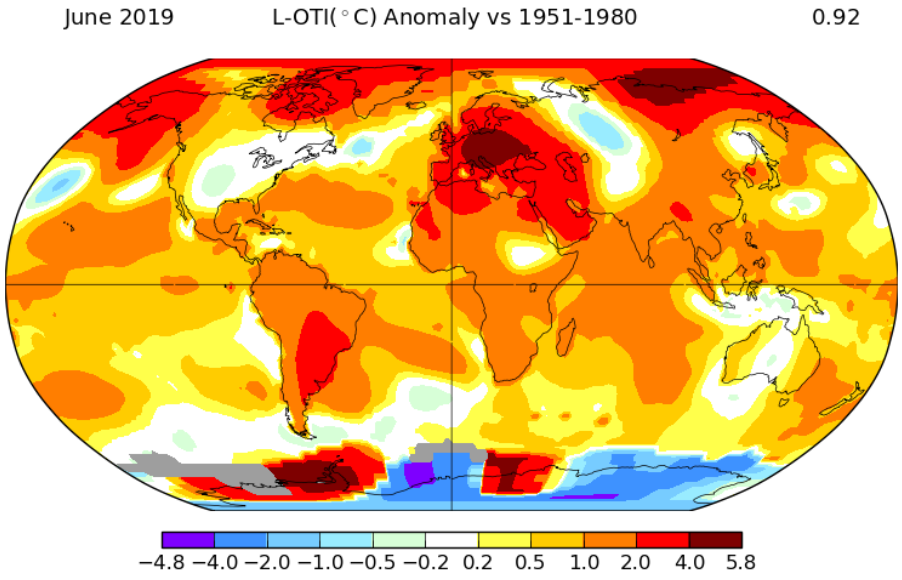

Figure 1: Land-Ocean Temperature Index Anomaly in °C of June 2019 vs. 1951-1980 (NASA, 2019)

This Arctic amplification is especially affecting permafrost, which is underlying large areas in the Arctic and is subject to permafrost degradation.

Within a currently published special report (IPCC, 2019), a dramatic change of surface permafrost degradation is expected. In a business-as-usual scenario, about 75% of the permafrost area is

losing its permanently frozen conditions in the uppermost 3-4 m. Even in a mitigation scenario, more than one third is likely to be lost (Figure 2).

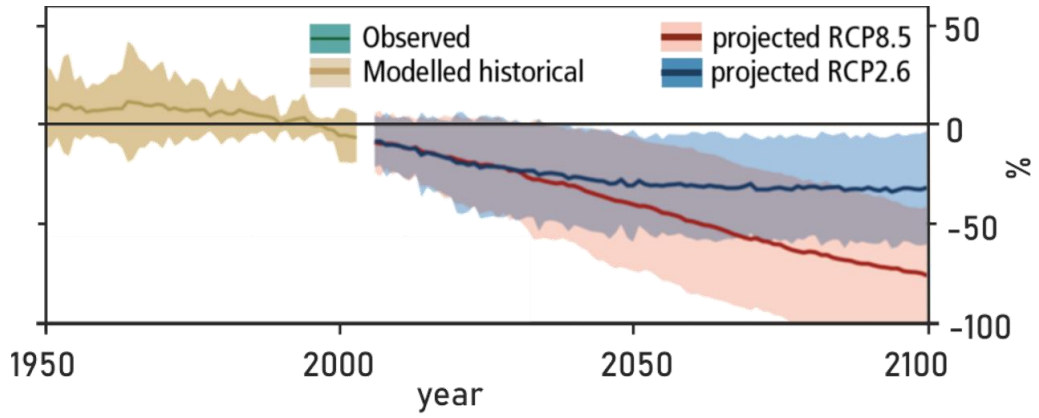

Figure 2: Observed and modelled historical changes in near-surface permafrost (within 3-4 m) area in the Northern Hemisphere since 1950 and projected future changes under low (RCP 2.6) and high (RCP 8.5) greenhouse gas emission scenarios (modified from IPCC, 2019).

Permafrost is a key element of the cryosphere and an important variable for the global climate. It stores large amounts of organic carbon and is affecting the stability of bedrock and ground sediments, when contained ground ice melts (Obu et al., 2019). It is estimated that almost twice as much carbon is locked in the permafrost region than there is currently in the atmosphere (Hugelius et al., 2014). When frozen ground thaws, freeze-locked organic carbon, nitrogen, and nutrients are decomposed by soil microbes and greenhouse gases are released into the atmosphere. This is accelerating climate warming as a positive feedback, also known as the permafrost-carbon feedback. In climate prediction models, these processes are not fully included yet and there are still uncertainties about the exact extent and the possible impact of permafrost and its degradation.

Consequently, it is essential to decipher permafrost decomposition and degradation processes, in order to forecast ongoing environmental changes in the Arctic region and their impact on global temperature trends. Furthermore, the quantification of stored organic carbon and its transport in permafrost landscapes is important, to estimate future effects and impacts of rapid permafrost thaw in the Arctic and globally.

In this thesis, Quaternary permafrost sediments were studied. The Quaternary is divided into the Pleistocene (2.588 million years to 11,700 years BP) and the Holocene (11,700 years BP to present).

Two sediment cores were taken in Central Yakutia, Siberia below two thermokarst lakes in the continuous permafrost zone. This region is highly affected by thermokarst processes and therefore an important study area regarding permafrost degradation and its consequences.

1.2 Objectives

The aim of my study is to assess the sedimentary and biogeochemical characteristics of permafrost lake deposits in Central Yakutia, Siberia. Regarding the objectives, two main parts are set for my thesis:

(1) The reconstruction of late Quaternary depositional processes in the study area by analysing the sedimentology of the deposits underlying the thermokarst lakes.
(2) Deciphering organic matter characteristics of the permafrost and thermokarst lake sediments from different development stages by analyzing the hydrochemistry and biogeochemistry to assess the relevance of the deposits for future degradation.

To understand future dynamics of permafrost landscapes, a reconstruction of the deposition and degradation history of the sediments is essential. With the help of sedimentological analyses, a reconstruction of former landscape development processes is possible. This reconstruction leads to a better understanding of past climate conditions, which is important for future climate predictions.
The amount of organic carbon and nitrogen can be investigated in different sediment layers, to quantify potential greenhouse gas emissions during thawing processes. Additionally important data is gained regarding carbon quantification.

The research questions, which are to be answered in this context, are:

a) Which depositional processes took place in the study area during past climate periods?
b) How much carbon is stored in the different sediment layers and the pore water of the drilling cores?

2. Geological and geographical background

In this chapter, characteristics of permafrost landscapes are described. Moreover the formation of thermokarst and thermokarst lakes is depicted.

2.1 Permafrost landscapes and periglacial environments

Permafrost is ground which stays at or below 0°C for two consecutive years (van Everdingen, 2005). It underlays about 12.8% to 17.8% of the Earth's exposed land surface including one quarter of the northern terrestrial hemisphere (Zhang et al., 2000) (Figure 3). Moisture in the form of water or ice can, but does not have to be present (French, 2017). The different permafrost zones (Figure 3) are characterized by the continuity and areal percentage of the frozen ground. They can be divided into the continuous permafrost zone (>90% permafrost coverage), the discontinuous permafrost zone (50-90% coverage), the sporadic permafrost zone (10-50% coverage) and the isolated permafrost zone (0-10% coverage).

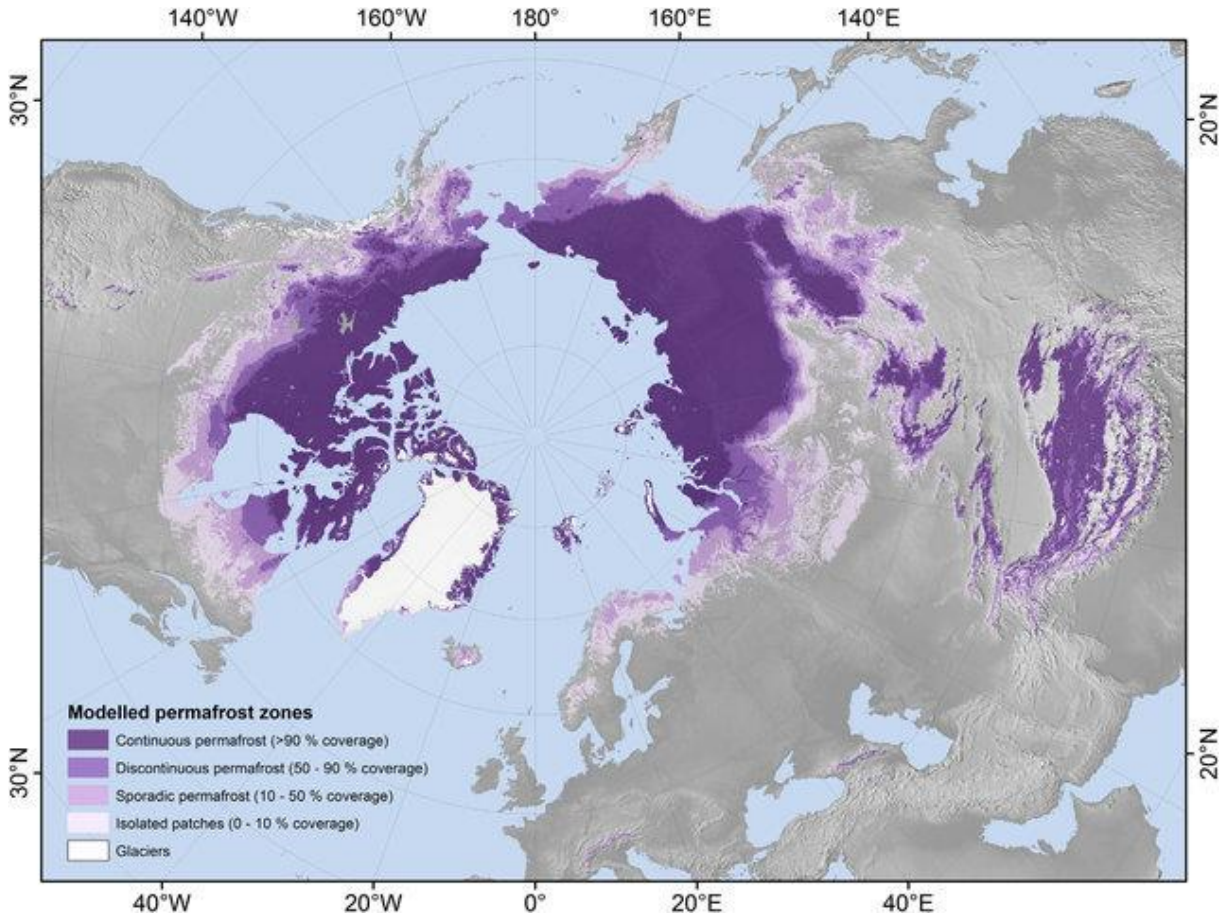

Figure 3: Permafrost distribution on the northern hemisphere (Obu et al., 2019)

The active layer is the seasonally unfrozen upper part of the permafrost, which thaws in summer and refreezes in winter. Its thickness varies between a few tens of centimeters to more than 2 meters in the continuous permafrost zone. In the discontinuous permafrost zone the active layer can reach several meters of thickness (Schuur et al., 2008). In the high Arctic of Russia, permafrost can reach depths down to 1500 meters (Kitover et al., 2016).

In big parts of permafrost landscapes ground ice is a major component of permafrost and in case of thawing ground and ice volume loss, ground subsidence is the result. Ground ice occurs in the form of pore ice, segregated ice, and intrusive ice. Pore ice is frozen pore water and is common in near surface permafrost and the active layer. Segregated ice forms especially in water saturated fine-grained sediments and is visible in the form of ice layers or lenses from a few millimeters to tens of meters thick. Intrusive ice results from water intrusion under soil water pressure. Ice wedges result from temperature-dependent expansion and contraction cracking and the related water infiltration during freeze- and thaw cycles (French, 2007). Ice-wedges form polygonal patterns, which are characteristic for periglacial environments. Ground ice can be either epigenetic (development after the enclosing sediment has been deposited) or syngenetic (forms at the same time as the enclosing sediments are deposited) (van Everdingen, 2005). In some areas ground ice can make up to 80% of the soil volume (Schirrmeister et al., 2011).

Permafrost stores large amounts of soil organic carbon, which is the remnant of plants and animals, accumulated in perennially frozen soil over thousands of years (Schuur et al., 2015). This carbon is vulnerable to remobilization, upon thawing in the course of global warming (Koven et al., 2015).

2.2 Permafrost degradation and thermokarst lake development

Permafrost is highly vulnerable to climate warming and degrades in different ways, depending on climate and the permafrost conditions itself, like ice content and ground temperature (Strauss et al., 2017). Main processes are the melting of ground ice linked to ground warming (Kurylyk et al., 2016), active layer deepening (Yi et al., 2018), thermal erosion along coastlines, rivers and lake shores (Günther et al., 2013), and rapid thaw linked to thermokarst.
Thermokarst is the process associated with the thaw of permafrost, linked to local or widespread collapse, subsidence, erosion, and instability of the ground surface (French, 2007). Thaw processes can be subdivided into thermokarst subsidence and thermal erosion. The first process is linked to the loss of water upon melting of ground ice and its removal by evaporation or drainage. The second describes the erosion by surface runoff and results in the formation of rills, gullies, and slumps (French, 2007).
In thermokarst landscapes, flat grassy treeless depressions with steep sides occur, which often contain shallow lakes. Such a depression is called Alas and can range from 0.5 to more than 100 km² in size (van Everdingen, 2005).

An important form of permafrost degradation is the formation and development of thermokarst lakes. They are defined as lakes that generate closed depressions (Alasses) formed by lake water induced settlement of ground, following thawing of ice-rich permafrost or the melting of massive ice (van Everdingen, 2005). They typically form in regions with an ice content above 30 Vol-% (Grosse et al., 2013). During the late Pleistocene-Holocene transition and in the Holocene Thermal Maximum, the formation of thermokarst lakes was widespread in the Arctic and sub-Arctic lowland regions with thermokarst characteristics (Walter et al., 2007). Today thousands of those lakes and remnant drainage basins can be found in the northern low land permafrost regions of Canada, Alaska, Scandinavia, and Russia (Grosse et al., 2013) (Figure 4). The satellite image of Central Yakutia, including the study site for this thesis, shows a thermokarst lake-rich land surface (Figure 5).

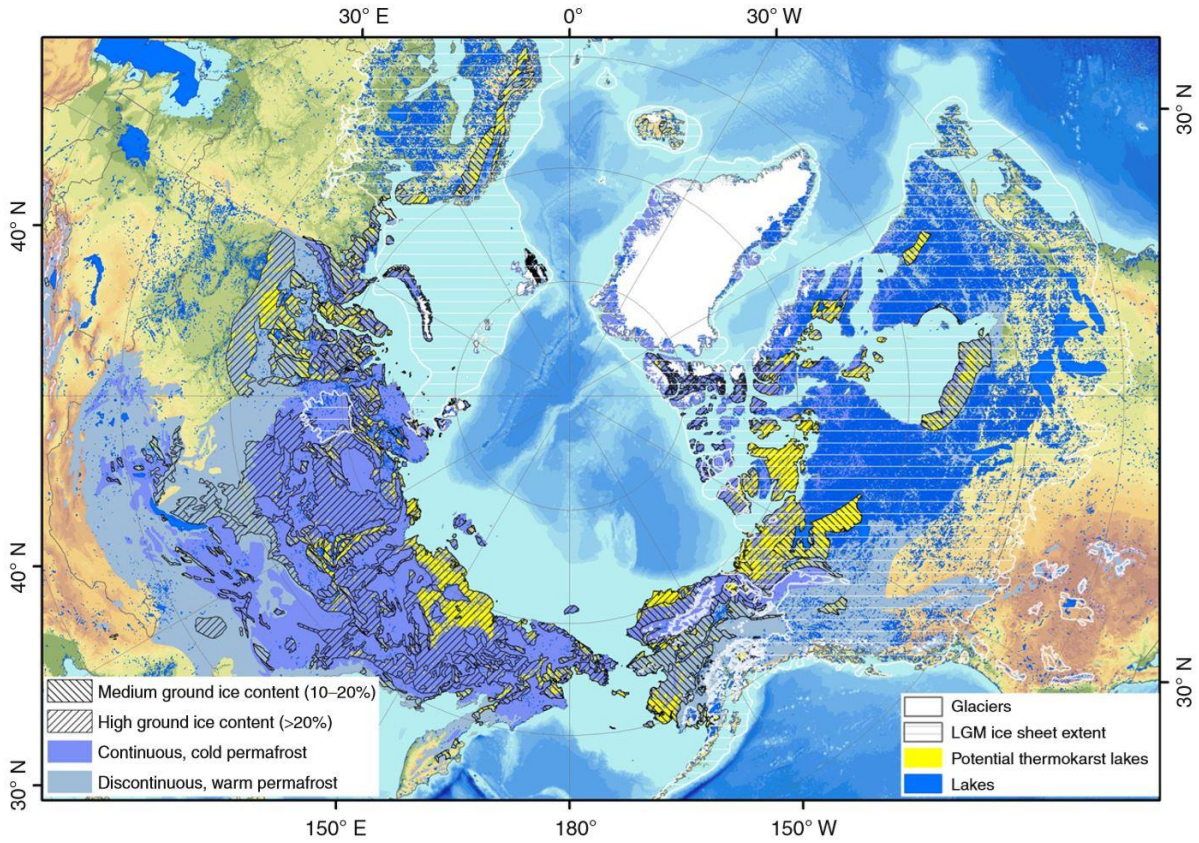

Figure 4: Pan-Arctic map of thermokarst lake regions (Grosse et al., 2013)

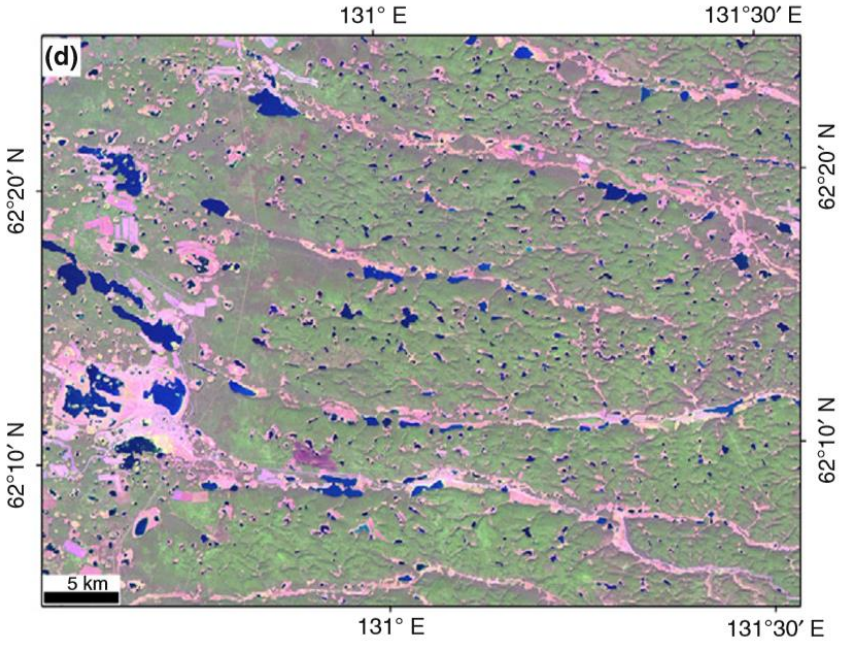

Figure 5: Landsat-5 TM satellite image showing a thermokarst lake-rich region in Central Yakutia, Siberia (RGB false-color composite using bands 5-4-3 at the same map scale. Landsat image. Reproduced from USGS EROS Data Center/NASA.) (From Grosse et al. (2013))

Thermokarst lake formation and growth is a form of deep and rapid permafrost degradation. The water surface strongly influences the albedo effect and consequently the surface energy balance (Jorgenson et al., 2010). Absorption of long-wave radiation, a lower albedo and a two to four times higher heat storage (compared to ice and dry ground) cause an increase of lake water and mean annual lake bottom temperatures at the water-sediment interface (Grosse et al., 2013). Thermokarst lakes are also an important source for atmospheric greenhouse gases, mainly carbon dioxide and methane. Anaerobic environments at the lake bottoms and the thawed sediments beneath the lakes cause the microbial decomposition of organic matter (OM) and methane production, which contributes to the current atmospheric carbon budget. The expansion of thaw lakes during the last decades was linked with a 58% increase in lake methane emissions, demonstrating an important feedback to climate warming (Walter et al., 2006).

During Yedoma sedimentation seasonal meltwater migrated into frost cracks and refroze, causing massive ice wedges. The formation of thermokarst lakes proceeded over the late Pleistocene and the Holocene. The ice wedges melted under the warmer Holocene climate, followed by ground subsidence.
The development of thermokarst lakes in ice-rich permafrost can be described in 4 main stages (Figure 6). In the first stage, ice wedges start to degrade, causing a hummocky surface (a,b). Following this, water can pool into degrading ice wedge troughs and small ponds can form, which then merge (c). As a result, small lakes are formed by the coalescence of several ponds and a talik is developing under the deepening lake (d). As a result, a large thermokarst lake with a deep talik has formed (e).

Talik formation is a fundamental process of thermokarst lake development. A talik is defined as a layer or body of unfrozen ground occurring in a permafrost area due to a local anomaly in thermal, hydrological, hydrogeological or hydrochemical conditions. If a talik is occupying a depression in the permafrost table beneath a lake, it is called a lake talik. Due to the heat storage effect of the lake water, the temperature of the talik sediments remains above 0°C (van Everdingen, 2005).
The thermokarst lake cycle also includes the drainage and the re-vegetation of lake basins. Such a drained basin is called Alas, where the aggregation of new permafrost and the reformation of ground ice is possible (Grosse et al., 2013).

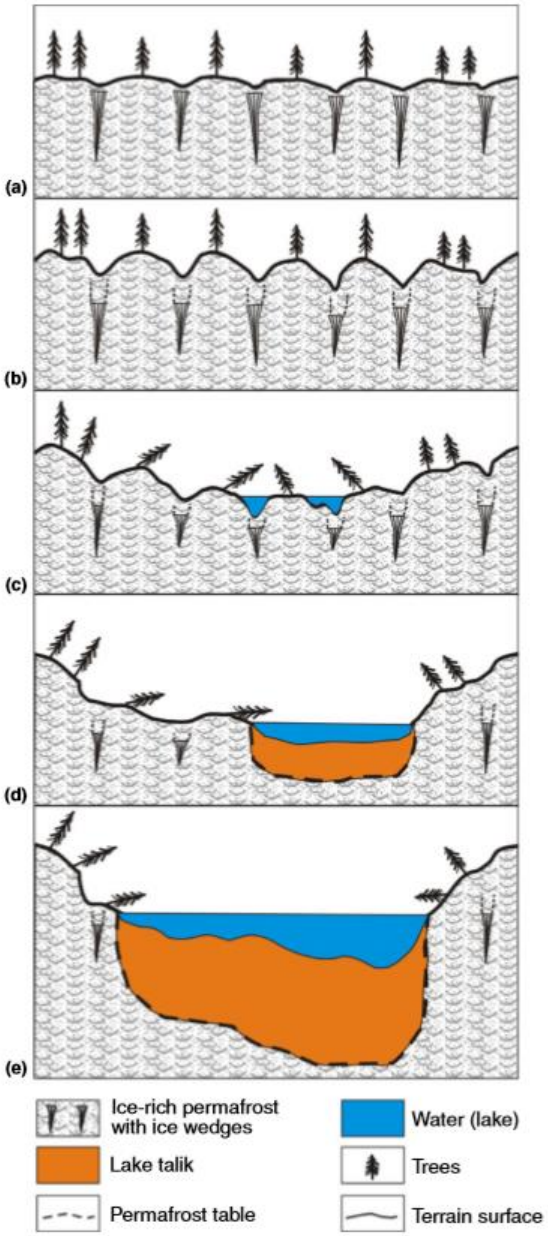

Figure 6: Main stages of the thermokarst lake cycle (Grosse et al., 2013).
Yedoma deposits with ice wedge formation and surface degradation (a,b), lake formation in ice wedge troughs and talik development (c,d), formation of large thermokarst lake with a deepening talik (e)

2.3 Yedoma

Yedoma is extremely ice-rich and silt-dominated syngenetic permafrost which originates from the late Pleistocene, covering large areas of Siberia and Alaska (Strauss et al., 2015). Alternatively the term Ice Complex is used for these deposits, matching their high ice content. In periglacial environments, Yedoma can reach 50 m in thickness and contains tall and wide ice wedges, which measure up to 3-4 meters in width on ground level (Kanevskiy et al., 2011).

Yedoma formation includes several stages which are assumed being differently intense in different regions of the Yedoma domain. For the north-eastern Siberian shelf region Schirrmeister et al. (2008) developed the following concept: In the first stage, windblown snow accumulates together with plant and mineral material in numerous perennial snow fields in topographic features of hills and low mountain ranges. In the following the formation of a concentrated detritus mat takes place, which results from repeated thawing of snow, material transport by meltwater and downslope accumulation of plant and mineral debris. The impact of intense freeze-thaw cycles and wet conditions support the formation of fine-grained material by frost weathering. The third stage is characterized by the discharge of clastic and organic detritus caused by snowfield meltwater runoff. Fine-grained material is distributed by alluvial, fluvial and partly aeolian transport. The Yedoma itself is subsequently formed during the concurrent process of sediment accumulation, ground ice segregation, syngenetic ice wedge growth, peat aggradation, cryosol formation and cryoturbation (Schirrmeister et al., 2008).

The extension of the Yedoma region is about 1 387 000 km^2 (Strauss et al., 2013). After its formation, which can be dated back to 55 ka BP and continued to 12 ka BP (Schirrmeister et al., 2013), Yedoma landscapes were widely affected by thermokarst and thermal erosion as a result of climatic changes from cool and dry to warm and wet conditions in the Pleistocene-Holocene transition (Kanevskiy et al., 2011). According to Strauss et al. (2013), approximately 70% of the Yedoma region is already affected by permafrost degradation and about 10% is covered with lakes and rivers and are underlain by unfrozen deposits.

The main source of OM enclosed in Yedoma deposits, is the late Pleistocene vegetation. Its origin, biogeochemical composition, and state of preservation determine the OM vulnerability (Strauss et al., 2017). Schirrmeister et al. (2008) cite average total organic carbon (TOC) values of 2-5 wt% for Yedoma landscapes.

The total frozen Yedoma region contains 211 + 160/ -153 Gt of organic carbon (OC), excluding the active layer and deeper OM deposits below Yedoma or frozen thermokarst deposits (Strauss et al., 2013). This OC pool is vulnerable to thaw, making it a relevant source of greenhouse gas emissions. Thawing of Yedoma deposits also causes deep ground subsidence, due to its high ice content.

2.4 Study area

The study area is located in the continuous permafrost zone of Central Yakutia, Russia (Figure 7a). Here, permafrost depths are reaching several hundred meters whereas the active layer reaches a depth of 1.0 m below forests and up to 2.0 m in grassland areas (Ulrich et al., 2017). The region is a low-relief landscape, characterized by many thermokarst basins (Alasses) and thaw lakes in different evolutionary stages (Ulrich et al., 2019) (Figure 8).

The region is characterized by a strong continental climate with low annual precipitation (223 ± 54 mm) and a mean annual air temperature of -9.8 ± 1.8 °C (calculated from Yakutsk weather stations' 1910-2014 data records by Ulrich et al., 2017). The vegetation in Central Yakutia is characterized by larch trees, with inclusions of pine and birch trees.

The drilling site is situated in the Lena-Aldan interfluve on the Abalakh terrace at approximately 200m above sea level. The investigated Yukechi Alas is located about 80 km southeast of the Yakutian capital Yakutsk (Figure 7b). Big parts of the interfluve region are covered by Yedoma deposits, containing up to 80 vol% ice, mainly in the form of syngenetic ice-wedges (Ulrich et al., 2019). Yedoma uplands and Alas basins indicate active thermokarst processes.

The drilling points for the lake sediment cores are located in the Alas lake (core YUK15-YU-L7) and the nearby Yedoma lake (core YUK15-YU-L15) (Figure 7c).

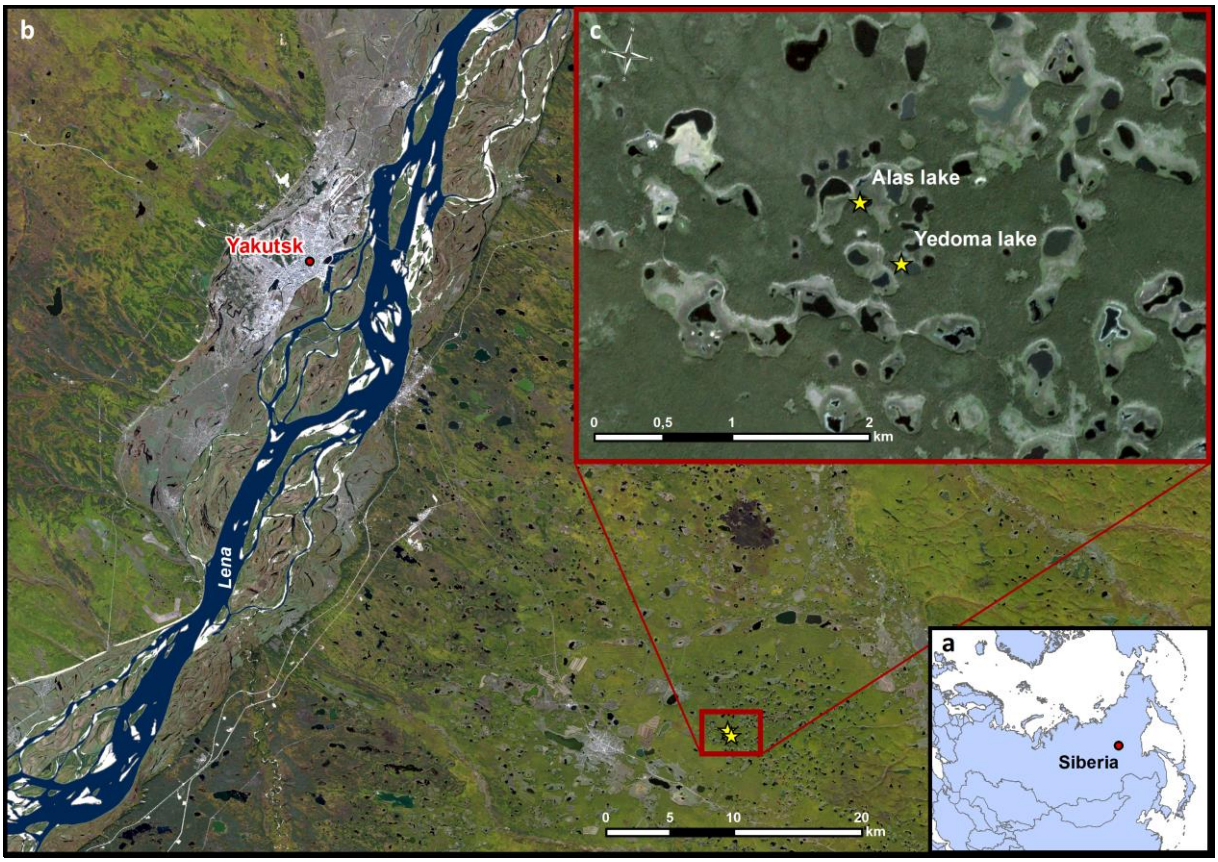

Figure 7: Overview of the study area in Yakutia, Siberia. (a) Location of Yakutsk in Siberia, Russia. (b) Study area on the Abalakh terrace near the Yakutian capital Yakutsk. (c) Yukechi Alas with the drilling points in the Alas lake and Yedoma lake

Figure 8: Field site impression in winter. A Yedoma rim covered with forest divides two Alas basins. The right hand basin with the hilly ground (thermokarst mounds with faster degraded ice wedges in between) drained into the left hand bigger basin through a drained channel, hardly visible in the picture behind the first row of trees (picture by J. Strauss, 2015)

3. Methods

In this section, the fieldwork settings and the obtained sediment cores are described. Furthermore, the laboratory working steps for the hydrochemical, biogeochemical and sedimentological analyses are explained.

3.1 Fieldwork

The lake sediment cores were obtained in March 2015 during a joint expedition of the Alfred - Wegener Institute Helmholtz Centre for Polar and Marine Research, the University of Leipzig and the Melnikov Permafrost Institute - Siberian Branch of Russian Academy of Science, Yakutsk, Russia. The fieldwork was part of two related research projects: the ERC project “Rapid Permafrost Thawing in a Warming Arctic and Impacts on the Soil Organic Carbon Pool” (PETA-CARB, 2013-2018) and the DFG project “Short and long-term thermokarst dynamics due to climate changes and human impacts in Central Yakutia, Siberia (2013-2016)”.

The sediment cores that are described in this study (Table 1) were drilled at the bottom of an Alas lake and a Yedoma lake. The Yedoma lake is an upland lake in undisturbed sediments, whereas the Alas lake lies 20 m lower in Holocene disturbed sediments (Figure 9).

The two cores were about 20 meters long. In the following, all depths are given as below ice-surface. In the boreholes, temperature loggers were installed which are able to record temperature data in different depths and are read out in changing intervals. In Table 1, the exact coordinates of the drilling points and the number of analysed samples are shown. In total, four cores were taken during the expedition. The two sediment cores underneath the lakes are analysed in this study. The other two cores from the Alas and a nearby Yedoma location were analysed by Windirsch et al. (submitted).

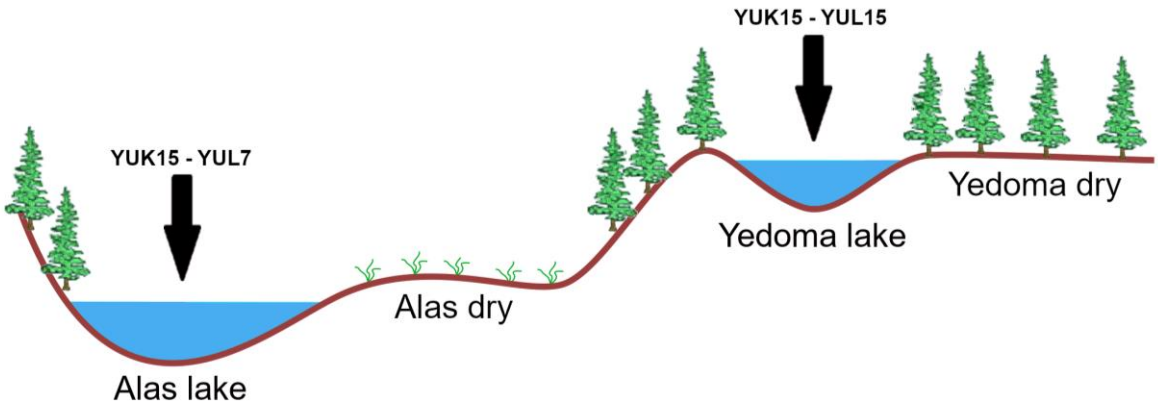

Figure 9: Cross-section of the study area with drilling points (modified from J. Strauss, 2015)

Table 1 Summary of lake sediment core characteristics

Drilling core ID	Landscape unit	Coordinates	Core depth / total recovery	Number of samples
YUK15-YUL7	Alas lake deposits	61.76397°N, 130.46445°E	2000 cm / 728 cm	19 samples
YUK15-YUL15	Yedoma lake deposits	61.76048°N, 130.47101°E	2146 cm / 1025 cm	50 samples
Total			**4146 cm / 1753 cm**	**69 samples**

Due to partly unfrozen sediment layers, big parts of the cores were lost during the drilling process. The applied URB2-47 drilling rig had no core catcher system, making it difficult to catch unfrozen sediments.

The gained core segments were stored in plastic bags and kept frozen until their analysis at AWI Potsdam. Figure 10 shows the approximate structure and core loss parts of both cores with pictures of halved core parts for different sediment layers.

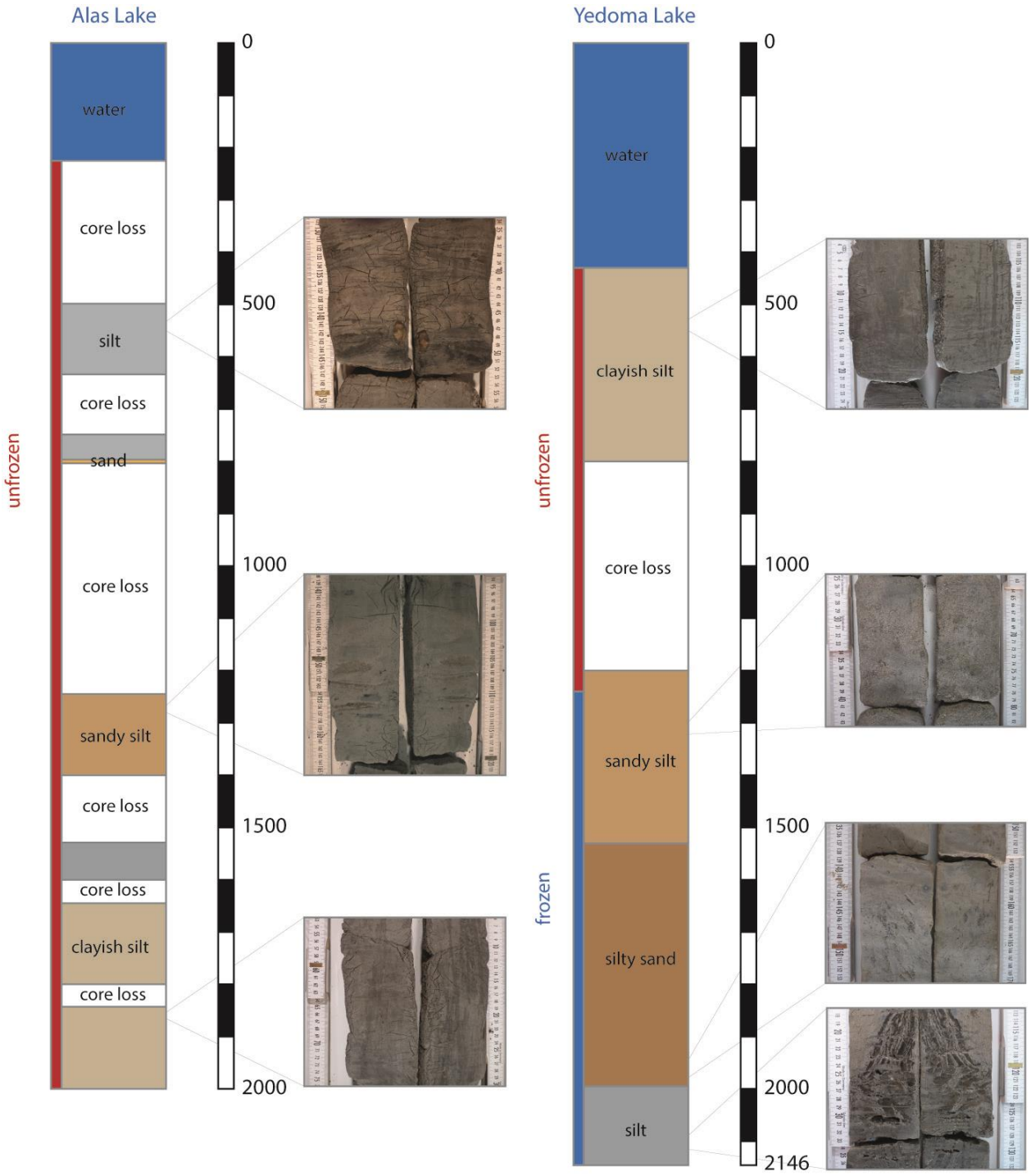

Figure 10: Core profiles of YUL15-YUL7 (Alas lake) and YUK15-YUL15 (Yedoma lake) with dominant sediment layers

3.2 Laboratory analysis - preparation

For the reconstruction of the late Quaternary landscape development, subsamples were taken from each of the sediment cores and the hydrochemistry, biogeochemistry and sedimentology were determined (Figure 11).

The subsamples were first analysed for water content and dissolved organic carbon content (DOC). From the pore water, the pH value and the electric conductivity were measured in several depths. Regarding the stable water isotope ratio, $\delta^{18}O$ and $\delta^{2}H$ were measured.

The sediment samples were analyzed for biogeochemistry and sedimentology. The biogeochemical analysis included the measuring of total carbon and total nitrogen (TC and TN), total organic carbon (TOC) and the ratio of stable carbon isotopes ($\delta^{13}C$). Magnetic susceptibility and grain size measuring were conducted during the sedimentological analysis.

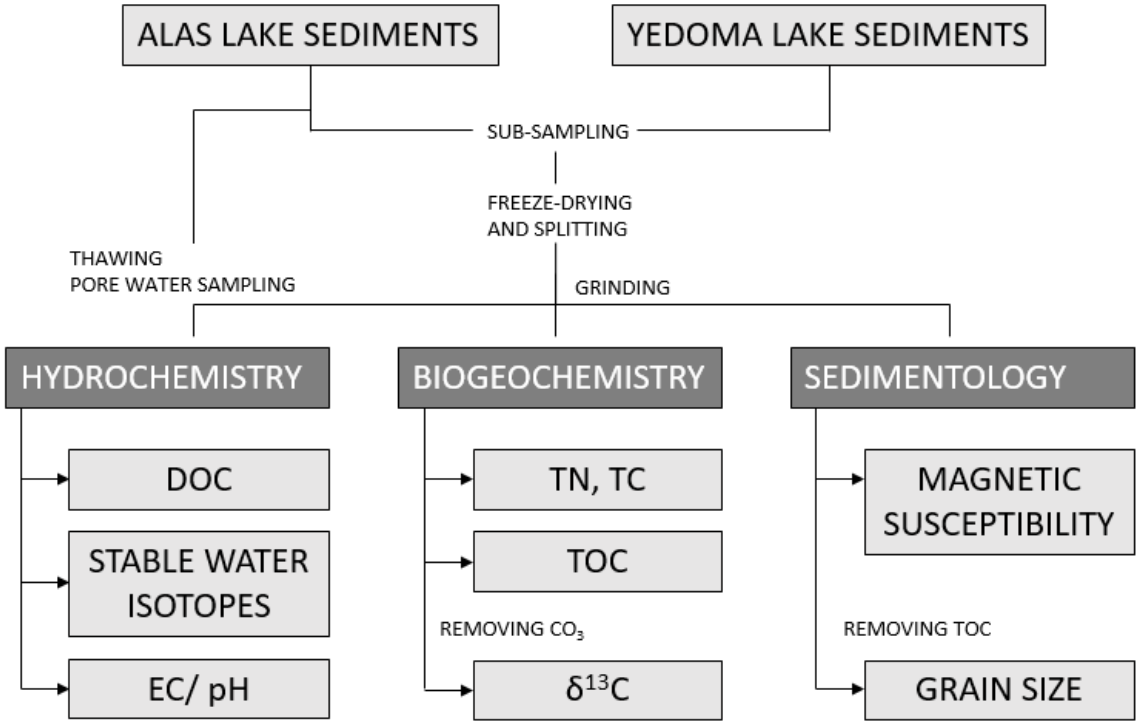

Figure 11: Laboratory analysing steps for hydrochemistry (including dissolved organic carbon, stable water isotopes, and electric conductivity and pH value), biogeochemistry (including total nitrogen and total carbon, total organic carbon and stable carbon isotopes) and sedimentology.

The frozen cores were first sawed into halves in the climate chamber at AWI Potsdam (Figure 12, 13). After cleaning the cut surfaces, the core was described visually and a photograph was taken of each part. One of the halves was kept for archive purposes. The "working half" was cut into subsample pieces at the selected depths. For the Alas core, samples were taken in intervals between 20 cm and 70 cm. For the Yedoma core intervals were more frequent with intervals between 10 cm and 40 cm. The subsamples were stored in plastic whirl bags, labeled and weighed.

For the biogeochemical and sedimentological analyses, the subsamples were freeze-dried after the pore water extraction. The opened whirl bags were covered with a thin tissue to prevent dust and small particles from being lost during the drying process. The samples were freeze-dried in the Zirbus Subliminator 3-4-5 at 0.2 bar and -40°C for two days. The samples were weighed again to determine the dry weight. Subsequently, the water content was calculated by deducting the dry weight from the wet weight.
For the calculation of the bulk density (BD), **Equation 1** was used. Hereby, the porosity of the soil (φ) describes the ratio between pore volume and the total volume. For the mineral density (ρ_s) a constant value of $2.65*10^3$ kg m^{-3} was assumed.

$$\mathrm{BD}\ [10^3\ \mathrm{kg\ m^{-3}}] = (\varphi - 1) * (-\rho_s) \qquad \textbf{Equation 1}$$

The dry samples were homogenized and split into two parts for the sedimentological and biogeochemical analysis. An additional replica was stored for archive purposes.
In preparation for the biogeochemical analyses, the samples were ground in agate beakers in a Planetary Mill Pulverisette 5 from Fritsch.

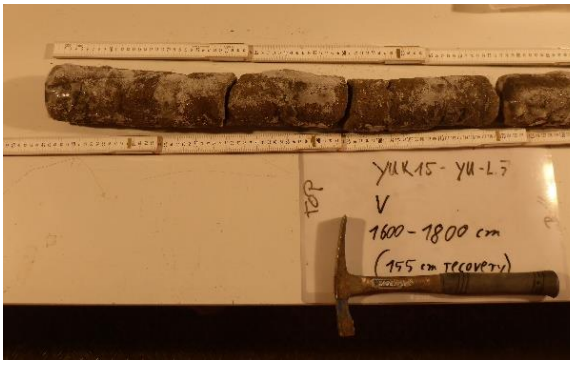

Figure 12: Frozen part of the Yedoma core YUK15_YUL15

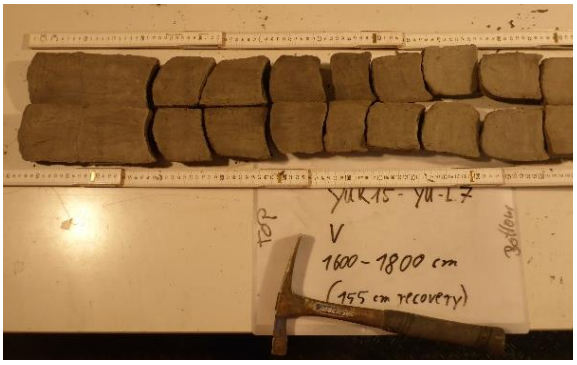

Figure 13: Halved and cleaned core part

3.3 Pore water extraction

Pore water was extracted from the sediments in order to measure dissolved organic carbon (DOC), stable water isotopes, electric conductivity, and pH-value. The subsamples were first thawed at a temperature of +4 °C. Following this, a Rhizone was inserted vertically in each of the thawed samples. Rhizones (*RHIZON soil moisture sampler MOM 10 cm)* represent artificial plant roots and consist of a small porous PE/PVC tube which is strengthened by a glass fiber wire with a diameter of 2.5 mm. The pore size of the membrane is between 0.12-0.18 µm, allowing a

filtration of particles bigger than 0.18 µm. A vacuum was applied to each Rhizone with the help of syringes. The extracted pore water was distributed into different subsample containers for follow-up analyses.

The water samples for the DOC analysis were acidified with 20µl concentrated (35%) hydrochloric acid (HCL) and were kept cool in a lab refrigerator at 4°C. 12 sediment subsamples did not hold enough water for pore water extraction.

3.4 Stable hydrogen and oxygen isotopes

Natural water consists of oxygen and hydrogen and is mainly formed by the stable water isotope $H_2{}^{16}O$, which makes up to 99.7%. Other stable isotope molecules are $H_2{}^{18}O$ (2‰), $H_2{}^{17}O$ (0.5‰) and $HD^{16}O$ (0.3‰), where H and D (deuterium) refer to ^1H and ^2H (Jouzel, 2003).
The distribution of water isotopes varies spatially and temporally in the atmosphere, in precipitation and consequently in the hydro- and cryosphere. (Jouzel, 2003). Lighter water isotopes evaporate more easily, whereas heavier isotopes remain in snow covers and seep into the active layer during melting.
Fractioning processes occur, due to the different physical properties of the molecules and the resulting different impact of evaporation and precipitation on lighter and heavier isotopes (Jouzel, 2003). Because of the modification by meteoric processes, the recharge waters in a particular environment will have a characteristic isotope signature.
The seasonal signal - which results from the strong correlation between temperature and stable isotopes in meteoric waters - can be used to date groundwater or make assumptions about the origin of the pore water (Clark and Fritz, 1997).

For the determination of the ratios of $^1H/^2H$ (δ^2H) and $^{18}O/^{16}O$ ($\delta^{18}O$), the water samples were measured in a Finnigan MAT Delta-S mass spectrometer. After Meyer et al. (2000), 5 ml of sample water were filled into 25 ml glass bottles, attached to a rack and placed in stirred water baths for homogenization of the temperature (18 ± 0.01°C).
Then, the samples were evacuated and hydrogen isotope measurements were conducted. The gases between water and H_2 fraction were equilibrated for the δ^2H value, using activated platinum condensed on a hydrophobic stick as a catalyst for the hydrogen isotope exchange. The method was repeated for the $\delta^{18}O$ measurement using CO_2 and water for equilibration (Meyer et al., 2000).
After equilibration, the samples were frozen in a cooling trap at -78°C to separate gas and water. The gas was then transferred into the sample bellow container. Sample and reference gases were alternately carried into the mass spectrometer. The water molecules are ionized and the deviation, which is caused by a strong magnet, is measured.
δ^2H and $\delta^{18}O$ values are calculated by the software ISODAT and displayed as per mill (‰) differences relative to the V-SMOW value (Meyer et al., 2000).

3.5 Dissolved organic carbon, electric conductivity, and pH-value

The dissolved organic carbon analysis contributes to carbon quantification in the core material of this study. The acidified samples (section 3.3) were used to analyse the dissolved organic carbon (DOC) as non –purgeable organic carbon (NPOC) in pore water of different depths of the core.

NPOC refers to organic carbon which is present in a sample in a non-volatile form. As this carbon gets lost in further analyzing steps (during the freeze-drying process), it has to be measured in advance. Measurements were mostly realized in dilution, due to small pore water sample amounts.

The DOC measurement was conducted with a Total Organic Analyzer TOC-VCPH/CPN from SHIMADZU. 2 ml of pore water were diluted with 10 ml of distilled water and filled into small test tubes. The tubes were placed into the auto-sampler of the analyzer. During the measurement, sparge gas was first bubbled through the sample and hydrochloric acid was added to remove inorganic carbon by converting it to carbon dioxide. The remaining organic carbon is measured by burning the sample and measuring the CO_2 concentration. To ensure the accuracy of the measurement, blank samples of ultra-pure water and standards with a known DOC concentrations were run before and after each measurement.
The electric conductivity and pH value measurements were conducted with a Multilab 540 (WTW) after the samples were warmed up to ambient temperature.

3.6 Total carbon, total nitrogen, and total organic carbon determination

To estimate the possible impact of stored carbon and nitrogen in permafrost soil on future climate and environmental changes and to reconstruct paleoenvironmental conditions, the total carbon (TC), total nitrogen (TN) and total organic carbon (TOC) content were analysed.
TOC is the organic material that originates from bioproductivity. TOC values reflect the variation in bioproductivity and organic matter accumulation. The ratio of total organic carbon and total nitrogen (TOC/TN or C/N) indicates the degree of decomposition of the OM, where low values represent stronger decomposed material and high values indicate less decomposed OM (Schirrmeister et al., 2011).
TC includes TOC, total inorganic carbon (TIC), bicarbonates and dissolved organic carbon (DOC).

TC and TN were quantified using the Elementar Vario EL III (Elementar Analysensysteme GmbH) (detection limit: 0.05% for carbon and 0.1% for nitrogen).
To quantify the amount of TC and TN, about 8 mg of homogenized sample material were encapsulated in duplicate into small tin capsules on a Sartorius micro MP3 scale. Tungsten (VI)-oxide was added as a catalyzer. For the background detection, a blank capsule was measured in the beginning and a calibration unit with control standards (Table 2) was run before every fifteen samples. The measurement is based on combustion chromatography, which implies the burning of samples at 950°C in an oxygen-saturated helium atmosphere. The elements of a sample (C, H, N and S) are oxidized into the gas phase and molecular N_2. Carbon dioxide (CO_2), elemental nitrogen (N_2), nitrogen oxide (NO) and nitrogen dioxide (NO_2) are formed. TC and TN values are calculated in wt%, as a result of the context between the amount of gas and the initial weight of the sample.

The TOC measurement was performed using the Elementar Vario Max C. This device follows a similar measurement principle as the TC and TN analyser, but at a combustion temperature of 580°C and a detection limit of 0.1 wt%.
The samples were weighted out on a different scale (Mettler Toledo XS105 Dual Range Analytical Balance) into steel crucibles. This was conducted twice for each sample. The explicit mass was

calculated, based on the TC values. At a carbon content lower than 2.3%, 95 to 100 mg were weighed into the crucibles. At a higher carbon content, 65 to 70 mg were used for measurements. Blank crucibles and control units were again run in between the actual samples for calibration.

Table 2 Standards for calibration and control units for TC and TN measurements

Standard	Calibration/ Control Sample
Sucrose (2x) EDTA 20 % (4) EDTA 10:40 (4x)	calibration
IVA 2176 (soil standard) EDTA 10:40 STSD 4 Mess-1 IVA 2152 BS2	control (after every 15 samples)

3.7 Stable carbon isotopes

The stable carbon isotope ratio ($\delta^{13}C$) describes the ratio of the heavy stable ^{13}C and the light stable ^{12}C atoms. The study of these isotopes can give an insight into biogeochemical processes regarding soil organic matter degradation and the degree of preservation (Andersson et al., 2012). As plant biomass reflects environmental conditions during the life period, paleoclimatic information can be stored in organic matter even beyond the lifespan of the plant.
The measuring unit is per mill (‰) and the ratio is compared to the C^{13}/C^{12} standard ratio, defined by the Vienna Pee Dee Belemnite (VPDB).

To prepare the subsamples for the $\delta^{13}C$ analysis, the carbonate had to be removed from the sediment, so that only the stable carbon isotopes from the organic carbon could be measured. This was done by treating the samples with hydrochloric acid. Approximately 1 gram of the ground sample was filled into an Erlenmeyer glass flask to which 20 ml of hydrochloric acid (HCl) were added. The flasks were placed on a hotplate for 3 hours at 97.7°C. The carbonate removal reaction during the cooking process is shown in **Equation 2**.

$$CO_3^{2-} + 2HCl \rightarrow CO_2 + 2Cl^- + H_2O \qquad \textbf{Equation 2}$$

After three hours, each flask was filled up to 100 ml with purified water. They were left standing for one day to wash out the chloride ions. After decantation of the water the flasks were filled up again. This procedure was repeated over three days until the pH value was 7 and the chloride content was under 550 ppm. To test the chloride ion content, Quantofix Chloride test stripes were used.

The decanted samples were filtered under vacuum using glass microfiber filters (GE Healthcare Life Sciences Whatman glass microfiber filters). After that, they were dried at 50°C in a drying oven and ground manually before being filled into prepared plastic jars.
The required sample weight was calculated by dividing 20 by the TOC value. The samples were weighed into small tin capsules on a Sartorius micro M2P scale with a maximum deviation of 0.02 mg.
The measurement of $\delta^{13}C$ was realized with a Flash 2000 Organic Elementar Analyzer by ThermoFisher Scientific, using helium as a carrier gas. The sample is combusted at 1020°C, transferring the OC to CO^2. The isotope ratio is determined relative to a laboratory standard of known isotopic composition. Calibration and standard capsules were run in between the measurements.
The $\delta^{13}C$ value was measured for samples with a TOC content above the detection limit only (31 out of 68 samples).

3.8 Mass specific magnetic susceptibility

The mass-specific magnetic susceptibility (MS) of a substance is a function of the concentration and type of magnetic minerals in the sample. The degree to which a substance perturbs a known magnetic field is measured (Begét et al., 1990). The MS of the sample material can give an impression of given stratigraphic sequences with a different magnetisability.

A Bartington Magnetic Susceptibility Meter Model MS2 (Bartington Instruments, UK) was used to measure the magnetisability of the samples in an external magnetic field in 10^{-8} m^3 kg^{-1}. This portable laboratory sensor has the ability to measure two different frequencies. The dual-frequency facility allows the detection of an important category of very fine ferromagnetic minerals, which are commonly found in soils and some rocks (Dearing, 1994).
The frequency used for measurement was 0.465 kHz, which characterizes a low frequency.

The mass-specific parameter X_{lf} is defined as the ratio of the volume susceptibility (κ) and the bulk density (ρ) which is shown in **Equation 3.**

$$X_{lf} = \frac{\kappa}{\rho} \qquad \textbf{Equation 3}$$

X_{lf} mass specific susceptibility for low frequency

κ volume susceptibility

ρ sample bulk density

3.9 Grain size analysis

The grain size characteristics of different sediment layers provide information about the depositional regime of the deposits. So, the grain size distribution can give insight into the kind of transportation, such as by wind, water or ice. For core YUK15-YU-L7 all subsamples were analysed for the given grain size distribution. For core YUK15-YU-L15, Unit 1 and 4 and every second subsample from Unit 2 and 3 were analysed.

To prepare the grain size analysis, organic matter had to be removed from the samples to ensure, only sediment particles and no organic particles were measured. For that, about 10 ml of each sample was put into a 400 ml beaker and was treated with 100 ml of 3% hydrogen peroxide (H_2O_2). Additionally, 4 drops of 32% ammonia were added, to reach a reactive starting pH value.
The beakers were put on a lab shaker, which was heated up to 60°C, for 2-3 weeks to catalyze the reaction of the organic matter. Five times a week, 10 ml of 30% H_2O_2 were added to each sample.
To stabilize the pH value between 6 and 8, concentrated acetic acid or ammonia were added.
After the organic matter was removed completely, the samples were washed with purified water to remove the H_2O_2. Before they were freeze-dried in plastic tubes, the samples were centrifuged, first in a Cryofuge 8500 i for ten minutes at 5050 RPM and subsequently in a Multifuge 3-SHeraeus 3-4 times at 4000 RPM for 15 minutes.
After manual homogenization, about 1 gram of each sample was weighed into 250 ml plastic tubules and half of a spatula of dispersing agent ($Na_4P_2O_7$, tetrasodium pyrophosphate) was added. Ammonia solution (10 ml NH_4OH mixed with 100 liters of water) was added and the samples were put on an overhead shaker overnight.
To ensure measurement concentrations between 5 to 15% turbidity, the samples were split into 8 homogeneous subsamples using a Fritsch laborette 27 Rotary Sample Divider. Additionally, the sample material was sieved to remove particles >1mm, which could damage the laser unit.
To analyse the grain size distribution, a Malvern Mastersizer 3000 (Malvern Instruments, UK) with an attached Malvern Hydro LV wet-sample dispersion unit was used. After providing a subsample to the dispersion unit, the Malvern Mastersizer measures three times and cleans automatically. The background scatter is measured and the sample is conducted to the measurement cell. If the deviation in grain size is less than 10% after measuring three subsamples, an average record is created which is representative for the whole sample. Subsequently, the statistical calculations for the grain size analysis were generated with the software GRADISTAT.

4. Results

In the following section, the laboratory results of the different analyses for the two lake sediment cores YUK15-YU-L7 and YUK15-YU-L15 are shown.

In chapter 4.1 the results for the stable water isotope analyses are plotted and described (Figure 14, 15). In chapter 4.2 the biogeochemical and sedimentological results are plotted over the mean sample depth in cm below surface level for both cores, showing the magnetic susceptibility, the different carbon characteristics, and the cumulated grain size distribution. The frozen or unfrozen state of the sediments is indicated (blue and red, respectively). For the grain size distribution, the volume percentage of each grain size for each sample is plotted in an extra diagram (Figure 17, 19). The raw data for the biogeochemical and sedimentological analyses are given in the Appendix.

4.1 Stable water isotope characteristics

Stable water isotopes (as $\delta^{18}O$ and $\delta^{2}H$ values) are plotted in relation to the Global Meteoric Water line (GMWL: y=8x+10) (Craig, 1961) for each core (Figure 14 and 15). The GMWL correlates with the average hydrogen and oxygen isotope composition of fresh terrestrial water on a global scale. It is a global average of many local meteoric water lines, each determined by local climatic factors, e.g. the origin of the vapor masses, secondary evaporation during rainfall and the seasonality of precipitation (Clark and Fritz, 1997). These factors affect the deuterium excess (d-excess = $dD-8*d^{18}O$) (Dansgaard, 1964) and the slope in the co-isotope diagram. The Local Meteoric Water Line of Yakutsk (LMWL: y=7.57x – 6.86 (Kloss, 2008)) is plotted additionally in blue with a lower slope and intercept in comparison to the GMWL. The Local Evaporation Line of Central Yakutia (LEL: 4.99x-61.41) is plotted in red and expresses regional evaporation effects on the waters in this area. To show the sample location within the core, values for $\delta^{18}O$ and d-excess are plotted over the core depth.

Regarding the Alas lake core YUK15-YU-L7 (n= 5), $\delta^{18}O$ and $\delta^{2}H$ values strongly differ from the GMWL and align with the LEL of Central Yakutia (Figure 14a). $\delta^{18}O$ values lie between -13.7 ‰ vs. VSMOW at 1302 cm mean depth BS and -12.9 ‰ vs. VSMOW at 1796 cm mean depth (Figure 14b). $\delta^{2}H$ values range from -129.0 ‰ vs. VSMOW (1649 cm BS) to -134.4 ‰ vs. VSMOW (1328 cm BS). The d-excess values vary between -24.9‰ and -27.6‰ and slightly decrease towards the bottom (Figure 14c).

The pore water samples of the Yedoma lake core YUK15-YU-L15 (n= 43) align with the GMWL, showing $\delta^{18}O$ values between -25.3 ‰ vs. Vienna Standard Mean Ocean Water (VSMOW) at a mean depth of 1316.5 cm below surface (BS) and -29.5 ‰ vs. VSMOW at 1931.5 cm BS (Figure 15a). $\delta^{2}H$ values lie between -184.2 ‰ vs. VSMOW (1316.5 cm BS) and -230.4‰ vs. VSMOW (1931.5 cm BS). In the upper part of the core, which was unfrozen down to 1200 cm BS, values align with the LEL of Central Yakutia. The $\delta^{18}O$ values generally decrease with depth, except in the bottom layer from 2064 cm BS to 2126 cm BS. Here values are slightly higher than in the overlying sections and are more similar to the upper layers (Figure 15b). For the d-excess, values lie between 5.12 (1957.5 cm BS) and 22.62 (1377.5 cm BS) and generally decrease with depth until 1957.5 cm BS, from where values are slightly increasing again (Figure 15c).

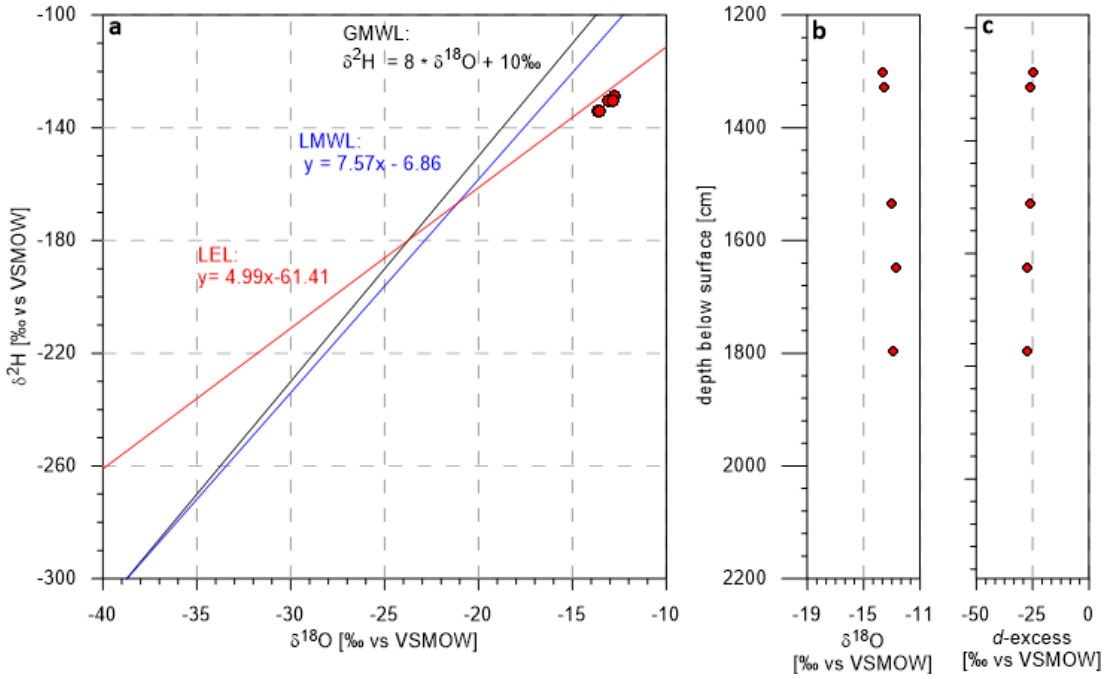

Figure 14: Stable water isotopes of YUK15-YU-L7 (Alas lake core). a: Hydrogen and oxygen isotopes, Global Meteoric Water Line (GMWL): y=8x (black), Local Evaporation Line (LEL) of Central Yakutia: y=4.99x-61.41 (red), Local Meteoric Water Line (LMWL) of Yakutsk: y=7.57x – 6.86 (blue); b: oxygen isotopes; c: d-excess values plotted over core depth

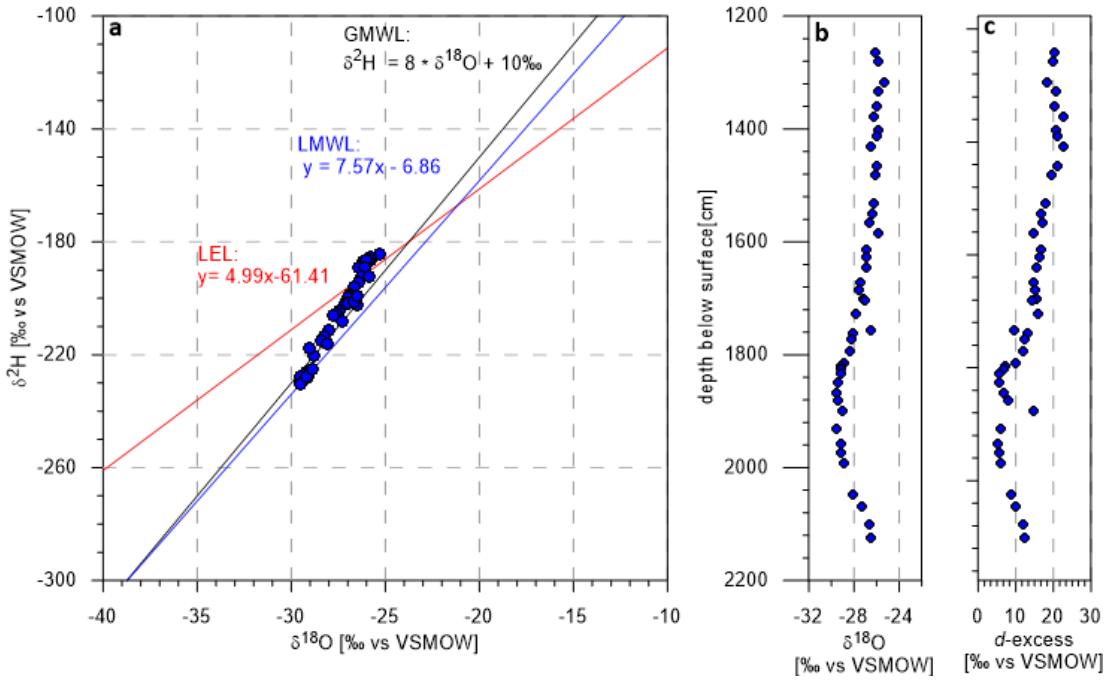

Figure 15: Stable water isotopes of YUK15-YU-L15 (Yedoma lake core). a: Hydrogen and oxygen isotopes, Global Meteoric Water Line (GMWL): y=8x (black), Local Evaporation Line (LEL) of Central Yakutia: y=4.99x-61.41 (red), Local Meteoric Water Line (LMWL) of Yakutsk: y=7.57x – 6.86 (blue); b: oxygen isotopes; c: d-excess values plotted over core depth

4.2 Carbon characteristics and sedimentology

In the following, the results for the carbon and sedimentological characteristics are described separately for each core.

4.2.1 YUK15-YU-L7

Core YUK15-YUL7 from underneath the Alas lake was completely unfrozen, resulting in a high core loss. The core is divided into 4 main units. Unit 1 reaches from 541 cm below surface (BS) to 778 cm BS and contains silty deposits. The next approximate 400 cm are core loss. Unit 2 contains more sand and reaches from 1245 cm BS to 1331 cm BS. The third Unit lies between 1395 cm BS and 1653 cm BS. At 1688 cm BS, Unit 4 starts with siltier deposits and higher carbon values (Figure 16).

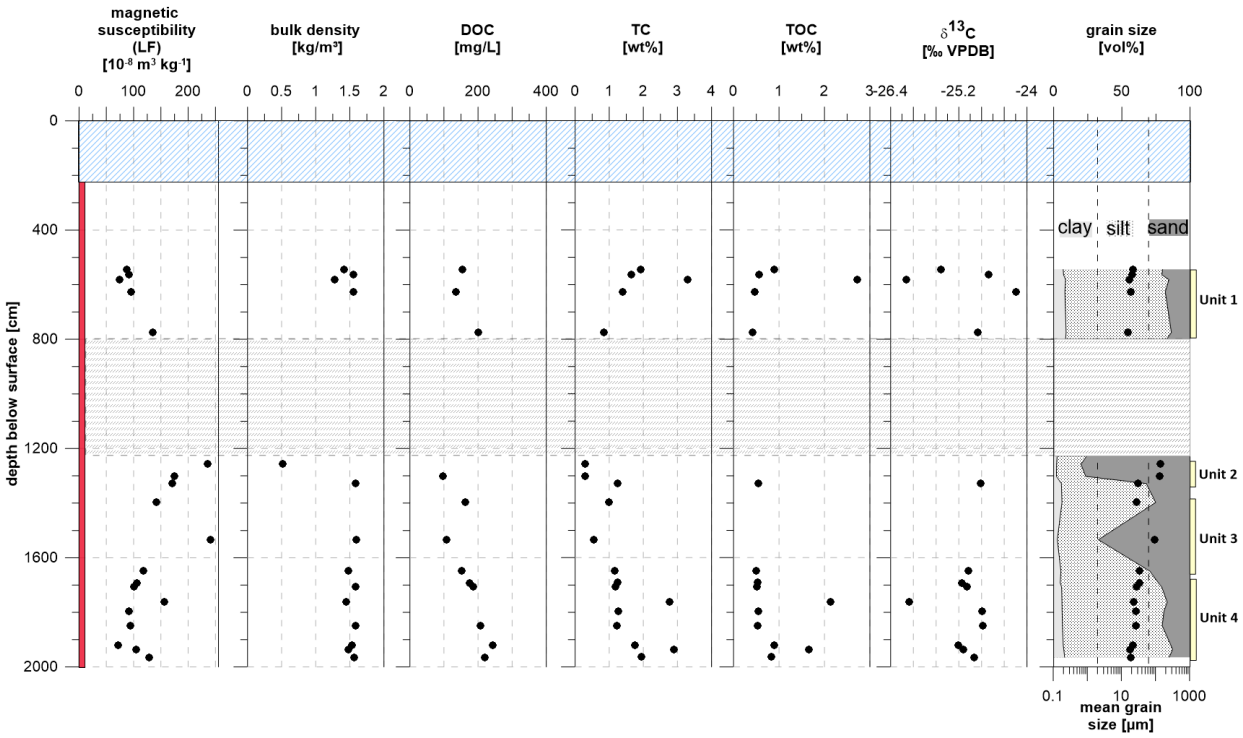

Figure 16: Laboratory results for YUK15-YU-L7 (Alas lake): magnetic susceptibility (low frequency), bulk density, dissolved organic carbon (DOC), total carbon (TC), total organic carbon (TOC), stable carbon isotopes (d13C) and grain size (cumulative and mean values)

Values for the magnetic susceptibility lie between 71.72 [10^{-8} m^3 kg^{-1}] at 1921.5 cm BS and 241.08 [10^{-8} m^3 kg^{-1}] at 1534 cm BS. The magnetic susceptibility increases in the first and the beginning of the second unit until 1257.5 cm BS. In Unit 3 and 4 values generally decreases until 1921.5. In the lowest part of Unit 4, values are slightly higher again.

The bulk density is relatively constant with values between 1.28 kg/m^3 and 1.59 kg/m^3 and a mean value of 1.44 kg/m^3. At 1257 cm BS there is an outlier with 0.52 kg/m^3.

DOC values vary between 96.6 mg/L and 242.4 mg/L with a mean value of 170.4 mg/L. In Unit 4 values are slightly higher than in the upper core parts.

The TC in Yuk15-YU-L7 ranges from 0.29% (1257.5 cm BS) to 2.90% (1936 cm BS). TC values show a peak in Unit 1 at 581.5 cm BS with 3.3% total carbon content. The first and third unit contain

relatively more total carbon than Unit 2. From the second to the fourth unit values are generally increasing with depth. TOC values lie between 0.42 wt% (775 cm BS) and 2.73 wt% (581.5 cm BS) and follow the TC trend. In the second and third unit, some TC values lie under the detection limit of the used device and could not be measured.

Due to low carbon contents, the $\delta^{13}C$ determination was only possible for the first and fourth unit and for one sample from the upper second unit. Values lie between -24.20 ‰ vs. VPDB and -26.12 ‰ vs. VPDB in Unit 1 and the top of unit 2. For Unit 4, samples have $\delta^{13}C$ values between -24.78 ‰ vs. VPDB and -26.07 ‰ vs. VPDB. In the upper part of the core, values are more scattered, whereas values in the fourth unit are quite similar, with one lower value at 1762.5 cm BS (-26.07 ‰).

Regarding the mean grain size, values follow a decreasing trend in Unit 1 and lie between 15.75 µm (775 cm BS) and 21.69 µm (544 cm BS). In Unit 2 the mean grain size decreases from 141.20 µm to 31.34 µm at the transition between a sand dominated fraction and the following silty fraction. In Unit 3 and 4 values lie between 18.31 µm (1936 cm BS) and 94.15 µm (1534 cm BS). At about 1500 cm BS there is another peak of sandy deposits.

The mean grain size maximum of 131.9 µm (1302 cm BS) is to be found in Unit 2 and the average within the core is located at 39.57 µm.

In YUK15-YU-L7, the clay content is quite low with values between 1.98 vol.% (1302 cm BS) and 9.12 vol.% (775 cm BS). The silt content represents the biggest part and varies between 17.93 vol.% at 1257.5 cm BS and 79.76 vol.% at 1936 cm BS. The sand content is highest in Unit 2 with 79.96 vol.% at 1257.5 cm BS and lowest in Unit 4 at 1936 cm BS.

The Alas lake core has a unimodal grain size distribution and shows poorly sorted material (mean sorting = 4.27). It is dominated by coarse silt deposits leaning towards sandy silt (Figure 17). In the upper and lower parts, coarse silt is dominant, whereas the second unit at 1257.5 cm mean depth shows medium sand deposits.

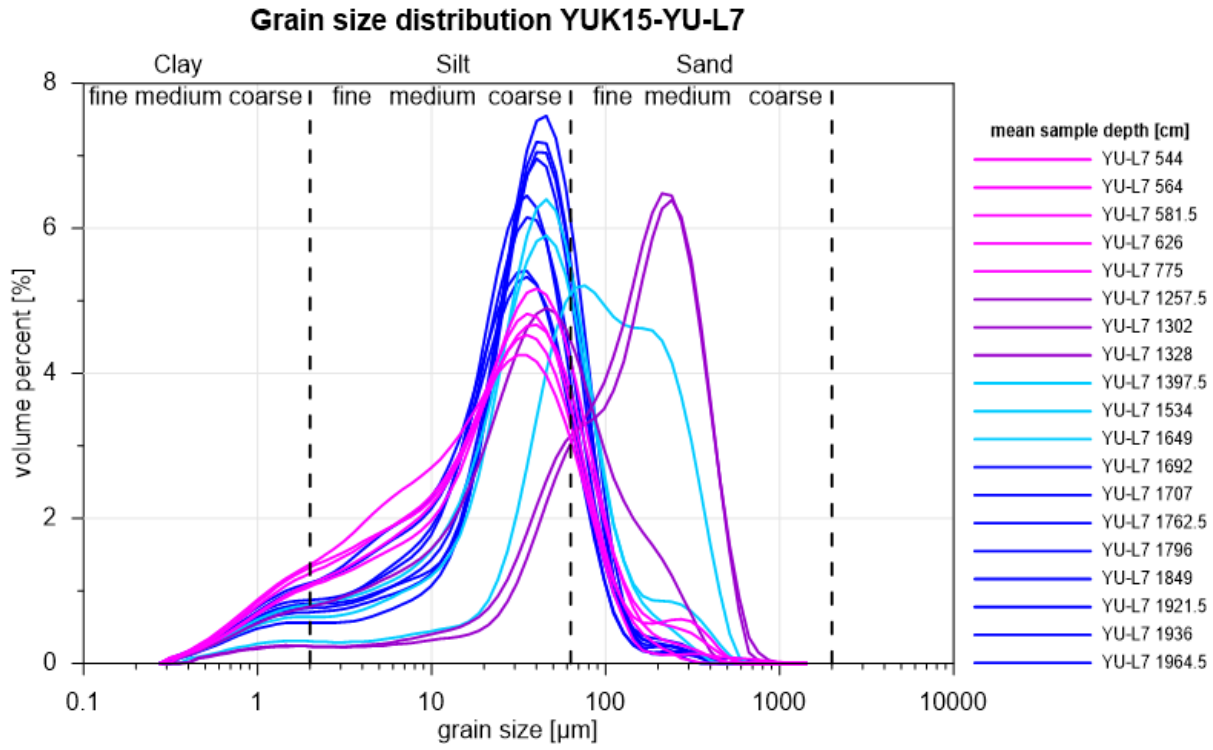

Figure 17: Grain size distribution for YUK15-YU-L7 (Alas lake). Colors correspond to the units defined in figure 16.

Another visualization for the sedimentary characteristics is the Shepard diagram, which is a three-component system showing the different grain size percentages of clay, silt, and sand. Each sample is plotted as a point within the diagram, according to its grain size composition. The samples of the two cores are plotted in red (YUK15-YU-L7) and blue (YUK15-YU-L15) in Figure 18. For the YUK15-YU-L7 core, there is a main cluster at the border of silt and sandy silt at about 75% silt and approximately 20% sand. A few samples contain nearly no clay and only little amounts of silt with approx. 18 to 30 vol% silt and up to 80 vol% sand.

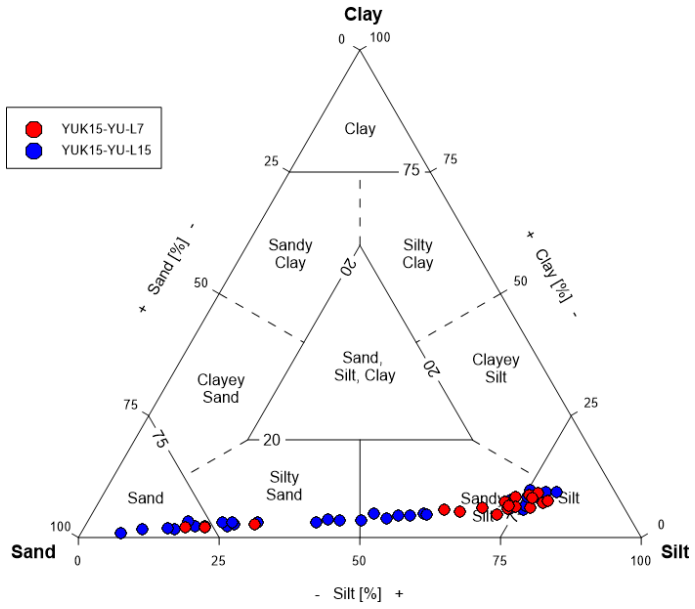

Figure 18: Sediment triangle after Shepard showing the grain size composition of YUK15-YU-L7 and YUK15-YU-L15 for each sample

4.2.2 YUK15-YU-L15

The YUK15-YU-L15 Yedoma lake core was unfrozen to a depth of approximately 1200 cm BS. It has a core loss section from 772 cm BS to 1222 cm BS and can be divided into four main units: Unit 1: 629 cm BS to 772 cm BS, Unit 2: 1222 cm BS to 1568 cm BS, Unit 3: 1568 cm BS to 1995 cm BS and Unit 4: 1995 cm BS to 2126 cm BS (Figure 19). The sediments between 772 cm BS to 1222 cm BS were lost during drilling.

In Unit 1, values for the magnetic susceptibility lie between 93.61 and 119.45. In the last three units, the magnetic susceptibility shows a generally decreasing trend and values lie between 67.35 at 2047 cm BS and 331.91 (1584 cm BS).

The bulk density in the first three sections varies between 1.13 kg/m^3 (1973.5 cm BS) and 1.57 kg/m^3 at 1584 cm BS. There are two outliers in Unit 3 at 1814 cm BS and 1820 cm BS with 0.09 kg/m^3 and 0.28 kg/m^3.

Regarding the DOC measurement, values are between 455.4 mg/L and 614.5 mg/L in Unit 1. In the second and third unit, values are increasing top-down and decreasing towards Unit 4. DOC values show a peak in the Unit 3 with a maximum of 1619.5 mg/L (1869 cm BS). The minimum of 93.6 mg/L is located in Unit 2 at 1294 cm BS.

The graphs for TC and TOC show similar trends in Unit 1 and 3, where the values are generally decreasing with depth. Unit 3 contains more total carbon than the other units.
TC values range from 0.17w% (1294 cm BS) to 3.56w% (1672 cm BS). In Unit 2 and 4, TC values lie under the detection limit and TOC could not be measured. TOC values range from 0.52 w% (1881.5 cm BS) to 2.45 w% (1672 cm BS). Hereby the maximum lies in unit 3.
$\delta^{13}C$ is higher (less negative) in the upper layers of the core. Values lie between -24.16 ‰ vs. VPDB at 796 cm BS and -26.11 ‰ vs. VPDB at 1672 cm BS. The lowest values are located in the upper part of Unit 3.

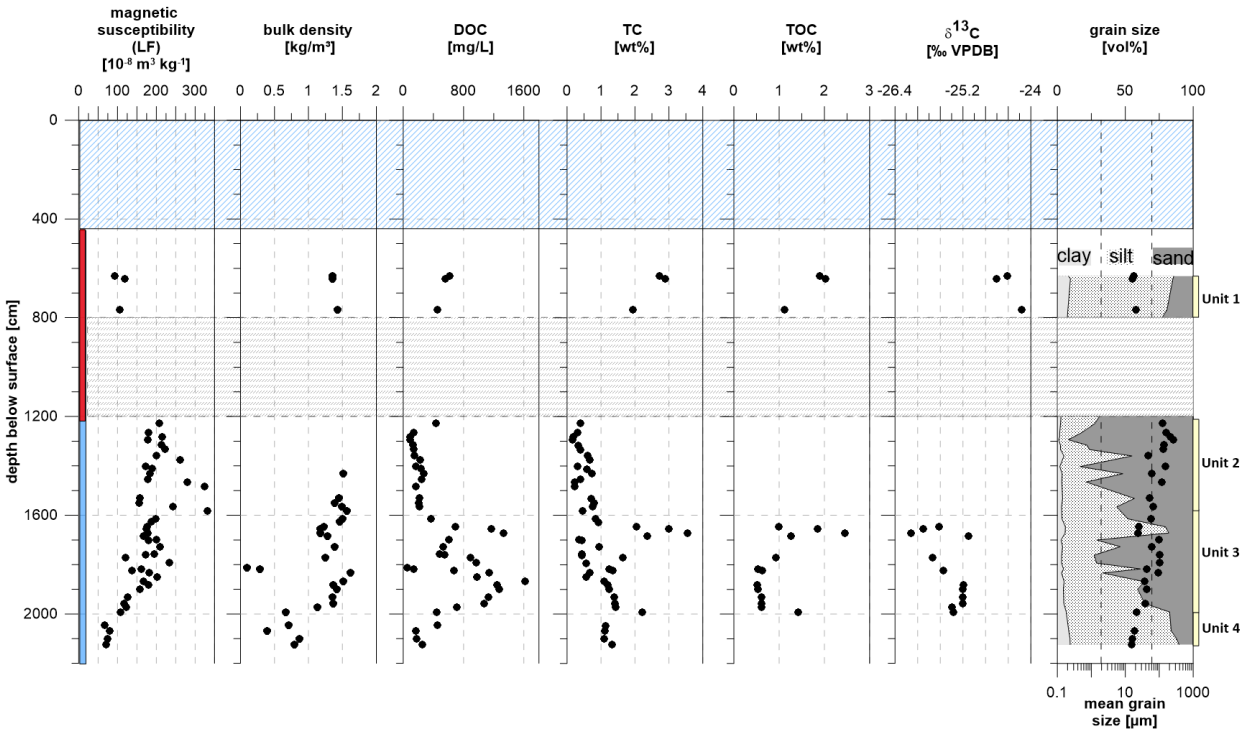

Figure 19: Laboratory results for YUK15-YU-L15 (Yedoma lake): magnetic susceptibility (low frequency), bulk density, dissolved organic carbon (DOC), total carbon (TC), total organic carbon (TOC), stable carbon isotopes (d13C) and grain size (cumulative and mean values)

In Unit 1, mean grain size values lie between 16.0 µm (642.5 cm BS) and 20.75 µm (1294 cm BS). In Unit 2 to 4, values show a decreasing trend with values between 15.82 µm at the very core end and 260.5 µm at 1294 cm BS. The fourth unit is mainly characterized by silty deposits, whereas the upper units (2,3) contain more sand with a silt shift at approx. 1650 cm BS.
The overall mean grain size is 77.14 µm. The clay content is relatively low with values between 0.9% (1294 cm BS) and 9.6% (642.5 cm BS). The silt content varies between 80.3% at the very bottom of the core and 7.1% at 1294 cm BS. The sections with the largest share of silt are Unit 1 and 4. The highest sand content is found in unit 2 with a maximum of 92.0% (1294 cm BS). After a silt shift at 1672 cm BS, there is another sand peak at 1762 cm BS with 72.9%. Unit 4 has the lowest sand content with 10.4% at 2124 cm BS.

Regarding the grain size distribution, the Yedoma lake core shows a unimodal behavior with poorly sorted material (mean sorting = 3.60). The second unit is dominated by medium sand, whereas the other units are characterized by coarse silt leaning towards sandy silt (Figure 20).

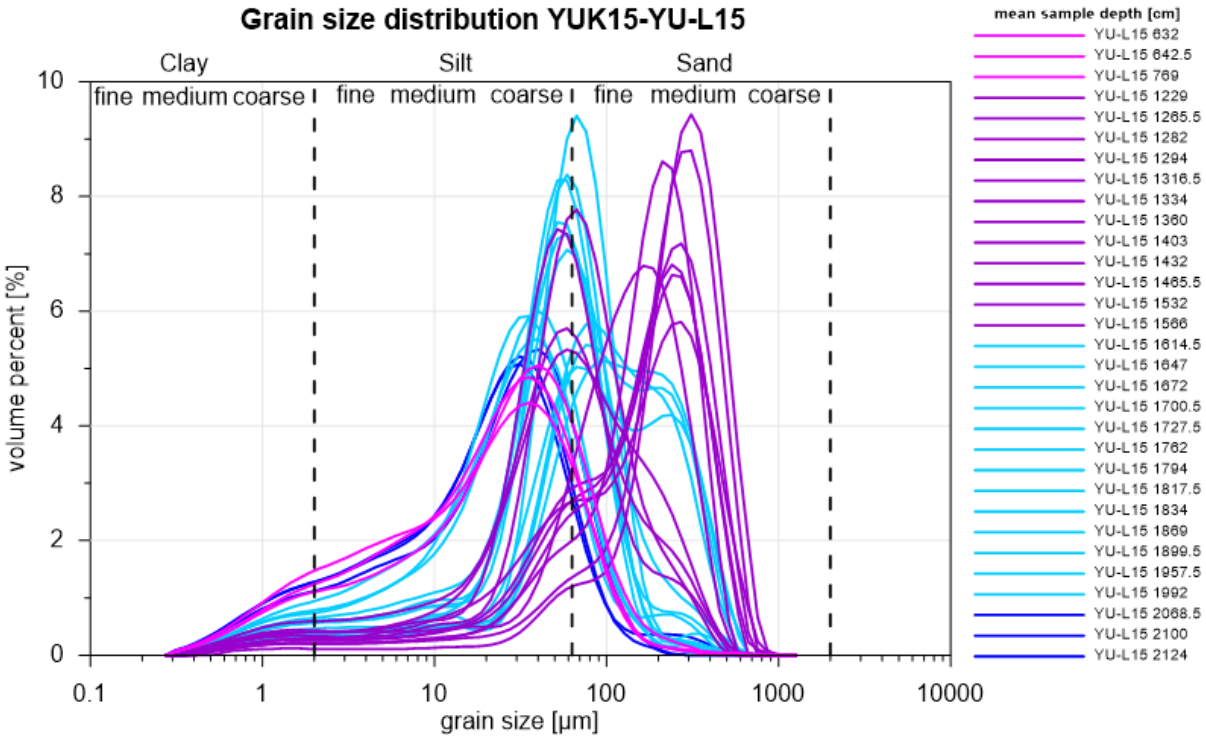

Figure 20: Grain size distribution for YUK15-YU-L15 (Yedoma lake). Colors correspond to the units defined in figure 19.

In the sediment triangle after Shepard (Figure 18), the YUK15-YU-L15 core shows a more differentiated grain size composition with the main cluster in the silt and sandy silt fraction. The measured samples for this core nearly cover the whole range between silt and sand with almost no clay (0.9 to 9.6 vol%) and up to 92 vol% sand in the second unit.

5. Discussion

The studied deposits are affected by the formation processes of thermokarst and thermokarst lake development, which are described in chapter 2.2. I found the sediment and biogeochemical characteristics depending on the different development stages. The Alas lake core YUK15-YU-L7 includes modern input, deeper thaw, and younger development characteristics, as it developed in the Holocene. The Yedoma lake core YUK15-YU-L15 shows older Pleistocene deposits which started being affected by lake water heat likely during the last century (personal communication M. Ulrich). The Alas lake itself is likely a remnant of a former big, partly drained Alas lake, but the thawing legacy of repeated thawing, refreezing, and thawing is not traceable with this multiproxy sedimentological approach.

The following discussion is split into 3 parts. In the hydrological part (5.1), the isotopic characteristics are discussed in regard to the environmental conditions during pore water infiltration. In section 5.2, the organic carbon characteristics are described, regarding its quantity and quality (future degradability). In 5.3, the depositional environment and its assumed formation will be discussed based on the analysed sedimentology.

5.1 Stable water isotopes, pore water, and ground ice

The two studied cores show different amounts of pore water which is linked to the different host sediments and their water storage capacity. With a mean value of 27.61% for the gravimetric water content, the Yedoma lake core contains more water/ice in comparison to the Alas lake core (mean value: 23.16%). A higher ice content and a lower bulk density in the lower half of the Yedoma lake core are linked to a higher vulnerability to thaw and ground subsidence. As the Alas lake core is completely thawed, no further ground subsidence is to be expected.

The composition of stable water isotopes in thermokarst lakes in the permafrost zone is mostly influenced by precipitation waters and occasionally by meltwater from the surroundings as well as by underlying permafrost (Wetterich et al., 2009). In comparison to North Yakutia, in Central Yakutia the influence by local temperatures and resulting evaporation effects on lake water $\delta^{18}O$ are stronger due to higher summer temperatures (Wetterich et al., 2008). The lake water is supposed to have a strong influence on the pore water isotope composition in case of ground thawing and infiltration of lake water.

Values for $\delta^{18}O$ and $\delta^{2}H$ of the Alas lake core YUK15-YU-L7 are higher than for the Yedoma-influenced thermokarst lake core YUK15-YU-L15. They represent a recent precipitation signal (slope= 5.7), caused by evaporative processes, as they strongly vary from the GMWL and align with the LEL.

The higher $\delta^{18}O$ and $\delta^{2}H$ values probably result from meltwater or water infiltration from the lake above, which is likely a strong evaporation system, as the core was completely unfrozen. The saturation with surface water results in relatively homogenous isotope signals. Regarding this, I was able to show that a subsurface water flow was possible after thaw, which has implications for local hydrology. In a warmer climate, new flow paths through former impermeable layers are possible.

For the YUK15-YU-L15 graph of $\delta^{18}O$ and $\delta^{2}H$, a slope of 11.5 is observed which is higher than that of the GMWL (slope=8). The differentiation of the single isotope values shows different fractions of the single core units. $\delta^{18}O$ and $\delta^{2}H$ values are the lowest from 1820 cm BS to 1973.5 cm BS, lying well below the GMWL, whereas those of the deepest part are slightly higher. The isotope

composition shows a larger range than in the YUK15-YU-L7 core, which could be indicative for warmer and cooler intervals during past climate periods.
A slope of greater than 8 in the co-isotope plot is rather seldom, as most water phase transitions (i.e. evaporation/condensation, freezing/melting) are characterized by slopes of 8 and lower. Since the linear correlation is based on a large number of samples covering a wide range of $\delta^{18}O$ and $\delta^{2}H$ values, it is likely that the slope is no artefact. A suitable assumption is a two-component mixing, e.g. the water in different depths originating from different water sources. These could be infiltration of surface water or precipitation from the top at different time periods (with rather heavy $\delta^{18}O$ values around -25‰, and high d-excess values around 20). The samples from the second unit downwards show rather light $\delta^{18}O$ values around 30‰ and a low d-excess of <10 which can be assigned to old, cold-stage permafrost deposits that probably have been frozen until today. This evidence of being frozen since deposition is important for interpreting the carbon inventories discussion in the next chapter.
In the upper unfrozen part of YUK15-YU-L15 values align with the LEL and could be indicative for rather initial, unfractionated water. The s-shaped curve of $\delta^{18}O$ over depth indicates a mixing between two endmembers (heavy delta values and high d-excess vs. light delta values and low d-excess). Meyer et al. (2002a) observed a similar pattern in the co-isotope diagram and interpreted a two-component mixing between Holocene and Pleistocene waters (or ice). In line with this interpretation, the YUK15-YU-L15 record could reflect cooler and warmer periods during past accumulation and water infiltration processes.

5.2 Carbon

The quantification of the OM, which might be vulnerable to rapid permafrost thaw, is important to estimate the relevance of the study site regarding potential future greenhouse gas release.
The TOC for YUK15-YU-L7 has a mean value of 0.92 wt%, whereas the mean value for YUK15-YU-L15 lies at 1.13 wt%. These relatively low values fit to previous studies carried out on thermokarst basins in central Yakutia (Ulrich et al., 2019). They generally contrast with TOC values in Siberia and Alaska of 3.0+1.6/-2.2 wt% and 6.5+3.9/-5.0 wt% of thermokarst deposits (Strauss et al., 2013) but fit well with results of cores taken close by (Windirsch et al., submitted). In both cores, TOC correlates with grain size. Extreme low TOC values are linked to coarser sediments, whereas higher TOC values are found in siltier layers.

According to Lenz et al. (2016b), thermokarst lakes are characterized by low primary production under Arctic climate, which could influence the TOC values. Another explanation for the low TOC content can be a strong post-sedimentary organic carbon decomposition during a thawed state, whereas high TOC values could reflect low OM degradation in the past (Strauss et al., 2015). The stable water isotope values for the lower part of core YUK15-YU-L15 strongly vary from the LEL, indicating that at least this part has not been thawed since accumulation. Therefore a high OM degradation is unlikely.
Another explanation for the low TOC values, even in constantly frozen sediment layers, can be a low organic carbon input. As the study site is located in a river interfluve, fluvial sedimentation processes of Lena tributaries led to the accumulation of coarser sediments. On these, plant growth was hampered by substrate quality and e.g. disturbance frequency and the OM input was restricted. The higher TOC values in core YUK15-YU-L15 in the third unit are the result of changed accumulation processes.

The TC values contain the organic and inorganic carbon and are also comparatively low. For YUK15-YU-L15, TC values correlate negatively with the mean grain size values. This shows the lower carbon content in sandier shifts which contain more carbonate and less carbon. Regarding this, DOC, TOC and TC values show local peaks at the silt shift at 1672 cm BS. An explanation for lower carbon values in sandy deposits might be their larger pores, causing a higher wash-out rate of organic matter.
DOC values of YUK15-YU-L15 are generally higher than those of YUK15-YU-L7 which can indicate different washout rates over time. Higher DOC values can also result from freshly thawed input from newly thawed permafrost, which is more likely.
Further OM decomposition processes within the talik below the thermokarst lakes are possible and traceable using the $\delta^{13}C$ isotopes. $\delta^{13}C$ values give information about plant metabolism, as they are generally very similar to those of the former vegetation. Very low (more negative) $\delta^{13}C$ values can be interpreted as an indication of less-degraded OM, while higher (less negative) $\delta^{13}C$ values are linked to stronger decomposition processes (Meyers, 1994).
For the upper part of the Yedoma lake core, isotopes show higher (less negative) values, indicating a lower quality and higher decomposition (Strauss et al., 2015). The higher quality signal in the upper part of the Alas lake core (-26.12‰) is likely a modern input. As mentioned before, a complete degradation of the carbon in Unit 2 and 4 of YUK15-YU-L15, where carbon isotope measurements were not possible, is very unlikely and thus not a degradation signal.
A carbon-nitrogen ratio was not calculated, as only two samples of YUK15-YU-L15 had total nitrogen contents above the detection limit of >0.1 w%, resulting in a CN-value of 16.02 (1684.5 cm BS) and 14.01 (1992 cm BS). As very low nitrogen estimates come with a high uncertainty, a detailed interpretation is not valid.

5.3 Sedimentology and deposit origin

By the analysis of the grain size distribution, assumptions about the source of the sediments and main deposition processes can be made. For YUK15-YU-L7, the sediments mainly consist of silt and sandy silt and the sediments are poorly sorted, which indicates short transport paths or an overlay of different formation processes like aeolian and alluvial/ fluvial processes (Ulrich et al., 2019). As the study site is located in the Lena-Aldan interfluve with many on-site outlet channels, alluvial and fluvial sedimentation is more likely than aeolian processes. The sandy deposits in the second unit of the core are likely related to fluvial sedimentation processes. The sand shift in unit 3 could be caused by a past lake drainage event, were coarser sediments remained after the removal of silty deposits.
Core YUK15-YU-L15 is mainly characterized by silty sand, but also includes sand, sandy silt and silt. As the main part is dominated by sandy deposits, fluvial sedimentation processes are likely, as large particles are mostly moved by surface water, like rivers or surface runoff from flooded areas. According to Ulrich et al. (2019), in general coarser sediments and especially the sand fraction within thermokarst lake basins point to shorter transport paths after erosion processes along lake shores.
In addition, the accumulation of coarser-grained sediments can also take place via longer high-energy transport by water.
The sandier sediment layers in the cores can be the result of increased water availability in rivers, resulting in a higher sand input due to higher transportation energy. The flow velocity of the on-

site tributaries is also an influencing factor, as higher velocities allow the deposition of larger particles.
The bulk density of both cores roughly follows the grain size. YUK15-YU-L7 shows slightly higher bulk density values than YUK15-YU-L15, which results from the higher sand content in the Yedoma deposits, which have a smaller water storage capacity. A higher pore water or ice content is a contributing factor for ground subsidence as a consequence of thermokarst degradation and increases the vulnerability to rapid permafrost thaw.
The similarities in the sediment composition of silt and fine sand in both cores point to a similar sedimentation regime for both sites in the past. The Alas results from thermal-altered Yedoma deposits, where the contained ground-ice thawed completely in the Holocene.
The different core units with finer and coarser sediments might be the result of different sedimentary regimes at this study site

The magnetic susceptibility is linked to the grain size in both cores, where sandier deposits match with higher MS values. In core YUK15-YU-L15, the mean MS value (174.9) is higher than the one of YUK15-YU-L7 (127,4). This might be the result of the reworking of Yedoma deposits under lacustrine conditions which causes the alteration of the MS signal. Lower MS values are the result of the degradation of the magnetizable minerals under reducing conditions and indicate an increase in lacustrine finer-grained detritus. Higher MS values point to an increased terrestrial coarser-grained input (Matasova et al., 2001; Ulrich et al., 2019).

Jongejans et al. (in prep.) dated several core samples of YUK15-YU-L7 and YUK15-YU-L15 via radio-carbon dating (Figures 21, 22). In the lower part of YUK15-YU-L7, the section from 1997-2000 cm BS is dated to approximately. 39.7 cal ka BP. The two dated samples above at 1745-1747 cm BS and 1559-1562 cm BS are older with ages >39 ka BP and >49.3 ka BP. The overlying layers were dated between >46.4 and 3.75 cal ka BP. The older shift in between might result from either cryoturbation during active thermokarst processes or sediment deposition from other areas. The upper two samples from 519-521 cm BS and 745-751 cm BS show values for Holocene sediments. The lower layers still originate from the Pleistocene. The older dates at approximately 1500 cm BS also conform to the grain size peak in the third unit of YUK15-YU-L7 and might be the result of a change of external sediment input.
The YUK15-YU-L15 core shows radio-carbon dates between >48.99 ka BP in the middle part at 1589- 1593 cm BS and 0.049 cal ka BP close to the surface at 589-601 cm BS. The core originates from the late Pleistocene, except the upper part (598-601 cm BS), which shows recent sediment deposits by modern lake input.

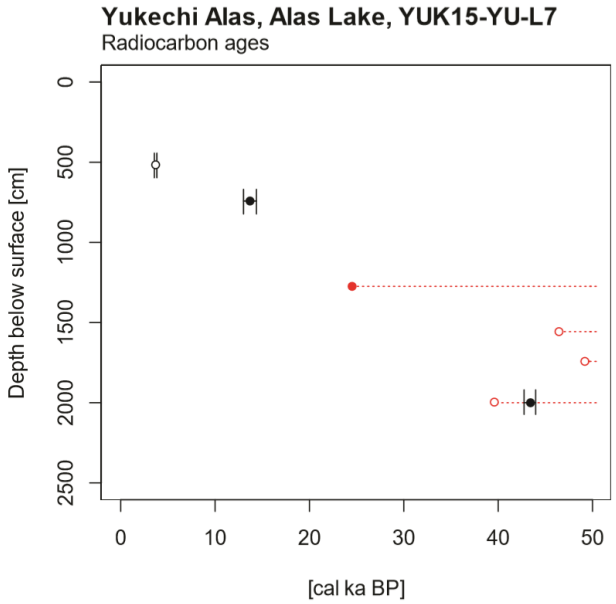

Figure 21: Radiocarbon dating for samples of YUK15-YU-L7(compiled by L.L. Jongejans, 2019)

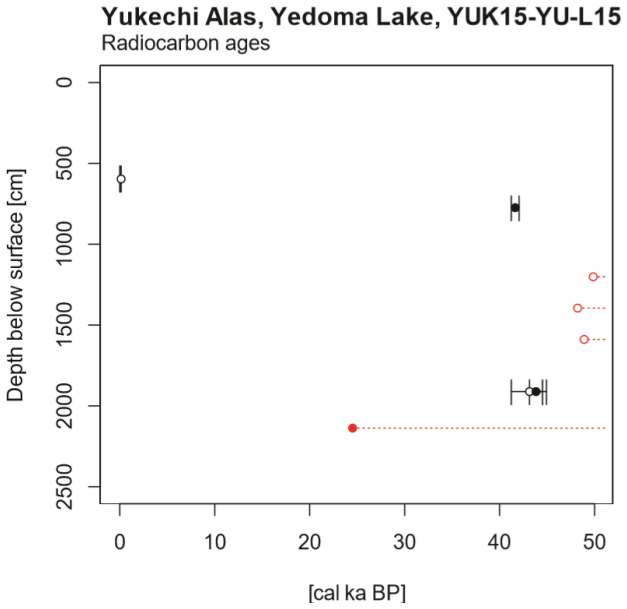

Figure 22: Radiocarbon dating for samples of YUK15-YU-L15 (compiled by L.L. Jongejans, 2019)

6. Conclusion

The sedimentological analyses were conducted for a better understanding of depositional processes and future dynamics of permafrost landscapes. The study of the organic matter characteristics helps to estimate the vulnerability of the thermokarst lake sediments to ongoing climate change. As the two study sites depict Yedoma deposits in different development stages, future changes of this thermokarst landscape can be predicted.

The first objective was to reconstruct the late Quaternary landscape development of the Yukechi Alas by analyzing the sedimentology of the deposits underneath the two thermokarst lakes. The Alas lake originates from a bigger drained thermokarst lake and the core YUK15-YU-L7 shows similar grain size characteristics to the Yedoma core YUK15-YU-L15. This supports the assumption that both cores originate from the same source of sediments. The silt and sand dominated deposits point to mainly fluvial sedimentation processes by receiving waters in the Lena-Aldan interfluve. Sandy shifts within the cores can be the result of higher streaming velocity or drainage events (YUK15-YU-L7), leaving only coarser sediments and causing the removal of fine material.

This fluvial sedimentation processes might also be the reason for the low carbon content of the deposits. In comparison to other Yedoma landscapes, the organic carbon values are extremely low and calculated carbon amounts (e.g. Strauss et al., 2012) cannot be supported. High OM decomposition rates are unlikely, as stable water isotopes for core YUK15-YU-L15 show low values, indicating that at least the lower part of the core was permanently frozen.

Therefore, the thawing of permafrost in this particular region might have a smaller input regarding the global permafrost-carbon feedback than previously thought. Nevertheless, the high ice content makes these deposits and Yedoma landscapes in general vulnerable to continuing permafrost thaw.

The number and size of permafrost lakes in the continuous permafrost zone is increasing (Smith et al., 2005) and especially in Central Yakutia, lake growth rates are significant (Nitze et al., 2017). The development of new and the expansion of existing thermokarst lakes in Yedoma regions is also connected to the enhanced release of methane, formed in lake sediments, which contributes to a changing climate (Walter et al., 2006). Global changing temperatures might lead to the complete thaw in the uppermost 3 m of the Central Yakutian permafrost and stored carbon can be released into the atmosphere, strengthening the arctic amplification.

Data availability: All data included in this study are available in the appendix and upon request to Jens Strauss (jens.strauss@awi.de)

7. References

Andersson, R.A., Meyers, P., Hornibrook, E., Kuhry, P., Mörth, C.-M., 2012. Elemental and isotopic carbon and nitrogen records of organic matter accumulation in a Holocene permafrost peat sequence in the East European Russian Arctic. J. Quat. Sci. 27, 545–552. https://doi.org/10.1002/jqs.2541

Begét, J.E., Stone, D.B., Hawkins, D.B., 1990. Paleoclimatic forcing of magnetic susceptibility variations in Alaskan loess during the late Quaternary. Geology 18, 40. https://doi.org/10.1130/0091-7613(1990)018<0040:PFOMSV>2.3.CO;2

Clark, I.D., Fritz, P., 1997. Environmental Isotopes in Hydrogeology. Lewis Publishers, New York.

Craig, H., 1961. Isotopic Variations in Meteoric Waters. Science 133, 1702–1703. https://doi.org/10.1126/science.133.3465.1702

Dansgaard, W., 1964. Stable isotopes in precipitation. Tellus 16, 436–468. https://doi.org/10.1111/j.2153-3490.1964.tb00181.x

Dearing, J.A., 1994. Environmental magnetic susceptibility: using the Bartington MS2 system. Chi Pub., Kenilworth.

French, H.M., 2017. The Periglacial Environment, 4. ed. Wiley-Blackwell.

French, H.M., 2007. The Periglacial Environment, 3. ed. John Wiley & Sons, Ltd.

Grosse, G., Jones, B., Arp, C., 2013. 8.21 Thermokarst Lakes, Drainage, and Drained Basins, in: Treatise on Geomorphology. Elsevier, pp. 325–353. https://doi.org/10.1016/B978-0-12-374739-6.00216-5

Günther, F., Overduin, P.P., Sandakov, A.V., Grosse, G., Grigoriev, M.N., 2013. Short- and long-term thermo-erosion of ice-rich permafrost coasts in the Laptev Sea region. Biogeosciences 10, 4297–4318. https://doi.org/10.5194/bg-10-4297-2013

Huang, J., Zhang, X., Zhang, Q., Lin, Y., Hao, M., Luo, Y., Zhao, Z., Yao, Y., Chen, X., Wang, L., Nie, S., Yin, Y., Xu, Y., Zhang, J., 2017. Recently amplified arctic warming has contributed to a continual global warming trend. Nat. Clim. Change 7, 875–879. https://doi.org/10.1038/s41558-017-0009-5

Hugelius, G., Strauss, J., Zubrzycki, S., Harden, J.W., Schuur, E.A.G., Ping, C.-L., Schirrmeister, L., Grosse, G., Michaelson, G.J., Koven, C.D., O'Donnell, J.A., Elberling, B., Mishra, U., Camill, P., Yu, Z., Palmtag, J., Kuhry, P., 2014. Estimated stocks of circumpolar permafrost carbon with quantified uncertainty ranges and identified data gaps. Biogeosciences 11, 6573–6593. https://doi.org/10.5194/bg-11-6573-2014

IPCC, 2019: Summary for Policymakers. In: IPCC Special Report on the Ocean and Cryosphere in a Changing Climate [H.-O. Pörtner, D.C. Roberts, V. Masson-Delmotte, P. Zhai, M. Tignor, E. Poloczanska, K. Mintenbeck, M. Nicolai, A. Okem, J. Petzold, B. Rama, N. Weyer (eds.)].

Jorgenson, M.T., Romanovsky, V., Harden, J., Shur, Y., O'Donnell, J., Schuur, E.A.G., Kanevskiy, M., Marchenko, S., 2010. Resilience and vulnerability of permafrost to climate changeThis article is one of a selection of papers from The Dynamics of Change in Alaska's Boreal

Forests: Resilience and Vulnerability in Response to Climate Warming. Can. J. For. Res. 40, 1219–1236. https://doi.org/10.1139/X10-060

Jouzel, J., 2003. 4.08 Water Stable Isotopes: Atmospheric Composition and Applications in Polar Ice Core Studies 31.

Kanevskiy, M., Shur, Y., Fortier, D., Jorgenson, M.T., Stephani, E., 2011. Cryostratigraphy of late Pleistocene syngenetic permafrost (yedoma) in northern Alaska, Itkillik River exposure. Quat. Res. 75, 584–596. https://doi.org/10.1016/j.yqres.2010.12.003

Kitover, D.C., van Balen, R.T., Vandenberghe, J., Roche, D.M., Renssen, H., 2016. LGM Permafrost Thickness and Extent in the Northern Hemisphere derived from the Earth System Model *i* LOVECLIM: LGM Permafrost Thickness and Extent using *i* LOVECLIM. Permafr. Periglac. Process. 27, 31–42. https://doi.org/10.1002/ppp.1861

Kloss, A.L., 2008. Water isotope geochemistry of recent precipitation in Central and North Siberia as a proxy for the local regional climate system.

Koven, C.D., Lawrence, D.M., Riley, W.J., 2015. Permafrost carbon−climate feedback is sensitive to deep soil carbon decomposability but not deep soil nitrogen dynamics. Proc. Natl. Acad. Sci. https://doi.org/10.1073/pnas.1415123112

Kurylyk, B.L., Hayashi, M., Quinton, W.L., McKenzie, J.M., Voss, C.I., 2016. Influence of vertical and lateral heat transfer on permafrost thaw, peatland landscape transition, and groundwater flow: PERMAFROST THAW, LANDSCAPE CHANGE, AND GROUNDWATER FLOW. Water Resour. Res. 52, 1286–1305. https://doi.org/10.1002/2015WR018057

Lenz, J., Jones, B.M., Wetterich, S., Tjallingii, R., Fritz, M., Arp, C.D., Rudaya, N., Grosse, G., 2016. Impacts of shore expansion and catchment characteristics on lacustrine thermokarst records in permafrost lowlands, Alaska Arctic Coastal Plain. arktos 2, 25. https://doi.org/10.1007/s41063-016-0025-0

Matasova, G., Petrovský, E., Jordanova, N., Zykina, V., Kapička, A., 2001. Magnetic study of Late Pleistocene loess/palaeosol sections from Siberia: palaeoenvironmental implications. Geophys. J. Int. 147, 367–380. https://doi.org/10.1046/j.0956-540x.2001.01544.x

Meyer, H., Derevyagin, A.Yu., Siegert, C., Hubberten, H.-W., 2002a. Paleoclimate Studies on Bykovsky Peninsula, North Siberia - Hydrogen and Oxygen Isotopes in Ground Ice. Polarforschung 70, 37–51.

Meyer, H., Schönicke, L., Wand, U., Hubberten, H.-W., Friedrichsen, H., 2000. Isotope studies of hydrogen and oxygen in ground ice - Experiences with the equilibration technique. Isot. Env. Health Stud 36, 133–149.

Meyers, P.A., 1994. Preservation of elemental and isotopic source identification of sedimentary organic matter. Chem. Geol. 114, 289–302. https://doi.org/10.1016/0009-2541(94)90059-0

NASA, 2019: GISS Surface Temperature Analysis (v4). https://data.giss.nasa.gov/gistemp/maps/index_v4.html (18.07.2019)

Nitze, I., Grosse, G., Jones, B., Arp, C., Ulrich, M., Fedorov, A., Veremeeva, A., 2017. Landsat-Based Trend Analysis of Lake Dynamics across Northern Permafrost Regions. Remote Sens. 9, 640. https://doi.org/10.3390/rs9070640

Obu, J., Westermann, S., Bartsch, A., Berdnikov, N., Christiansen, H.H., Dashtseren, A., Delaloye, R., Elberling, B., Etzelmüller, B., Kholodov, A., Khomutov, A., Kääb, A., Leibman, M.O., Lewkowicz, A.G., Panda, S.K., Romanovsky, V., Way, R.G., Westergaard-Nielsen, A., Wu, T., Yamkhin, J., Zou, D., 2019. Northern Hemisphere permafrost map based on TTOP modelling for 2000–2016 at 1 km2 scale. Earth-Sci. Rev. 193, 299–316. https://doi.org/10.1016/j.earscirev.2019.04.023

Schirrmeister, L., Froese, D., Tumskoy, V., Grosse, G., Wetterich, S., 2013. PERMAFROST AND PERIGLACIAL FEATURES | Yedoma: Late Pleistocene Ice-Rich Syngenetic Permafrost of Beringia, in: Encyclopedia of Quaternary Science. Elsevier, pp. 542–552. https://doi.org/10.1016/B978-0-444-53643-3.00106-0

Schirrmeister, L., Grosse, G., Wetterich, S., Overduin, P.P., Strauss, J., Schuur, E.A.G., Hubberten, H.-W., 2011. Fossil organic matter characteristics in permafrost deposits of the northeast Siberian Arctic. J. Geophys. Res. 116, G00M02. https://doi.org/10.1029/2011JG001647

Schirrmeister, L., Meyer, H., Wetterich, S., Siegert, C., Kunitsky, V.V., Grosse, G., Kuznetsova, T.V., Derevyagin, A.Yu., 2008. The Yedoma Suite of the Northeastern Siberian Shelf Region: Characteristics and Concept of Formation.

Schuur, E.A.G., Bockheim, J., Canadell, J.G., Euskirchen, E., Field, C.B., Goryachkin, S.V., Hagemann, S., Kuhry, P., Lafleur, P.M., Lee, H., Mazhitova, G., Nelson, F.E., Rinke, A., Romanovsky, V.E., Shiklomanov, N., Tarnocai, C., Venevsky, S., Vogel, J.G., Zimov, S.A., 2008. Vulnerability of Permafrost Carbon to Climate Change: Implications for the Global Carbon Cycle. BioScience 58, 701–714. https://doi.org/10.1641/B580807

Schuur, E.A.G., McGuire, A.D., Schädel, C., Grosse, G., Harden, J.W., Hayes, D.J., Hugelius, G., Koven, C.D., Kuhry, P., Lawrence, D.M., Natali, S.M., Olefeldt, D., Romanovsky, V.E., Schaefer, K., Turetsky, M.R., Treat, C.C., Vonk, J.E., 2015. Climate change and the permafrost carbon feedback. Nature 520, 171–179. https://doi.org/10.1038/nature14338

Smith, L.C., Sheng, Y., MacDonald, G.M., Hinzman, L.D., 2005. Disappearing Arctic Lakes. Science 308, 1429.

Solomon, S., Intergovernmental Panel on Climate Change, Intergovernmental Panel on Climate Change (Eds.), 2007. Climate change 2007: the physical science basis: contribution of Working Group I to the Fourth Assessment Report of the Intergovernmental Panel on Climate Change. Cambridge University Press, Cambridge ; New York.

Strauss, J., Schirrmeister, L., Grosse, G., Fortier, D., Hugelius, G., Knoblauch, C., Romanovsky, V., Schädel, C., Schneider von Deimling, T., Schuur, E.A.G., Shmelev, D., Ulrich, M., Veremeeva, A., 2017. Deep Yedoma permafrost: A synthesis of depositional characteristics and carbon vulnerability. Earth-Sci. Rev. 172, 75–86. https://doi.org/10.1016/j.earscirev.2017.07.007

Strauss, J., Schirrmeister, L., Grosse, G., Wetterich, S., Ulrich, M., Herzschuh, U., Hubberten, H.-W., 2013. The deep permafrost carbon pool of the Yedoma region in Siberia and Alaska: DEEP CARBON OF SIBERIA AND ALASKA. Geophys. Res. Lett. 40, 6165–6170. https://doi.org/10.1002/2013GL058088

Strauss, J., Schirrmeister, L., Mangelsdorf, K., Eichhorn, L., Wetterich, S., Herzschuh, U., 2015. Organic-matter quality of deep permafrost carbon – a study from Arctic Siberia. Biogeosciences 12, 2227–2245. https://doi.org/10.5194/bg-12-2227-2015

Ulrich, M., Matthes, H., Schirrmeister, L., Schütze, J., Park, H., Iijima, Y., Fedorov, A.N., 2017. Differences in behavior and distribution of permafrost-related lakes in Central Yakutia and their response to climatic drivers: YAKUTIAN THERMOKARST-LAKE BEHAVIOR. Water Resour. Res. 53, 1167–1188. https://doi.org/10.1002/2016WR019267

Ulrich, M., Matthes, H., Schmidt, J., Fedorov, A.N., Schirrmeister, L., Siegert, C., Schneider, B., Strauss, J., Zielhofer, C., 2019. Holocene thermokarst dynamics in Central Yakutia – A multi-core and robust grain-size endmember modeling approach. Quat. Sci. Rev. 218, 10–33. https://doi.org/10.1016/j.quascirev.2019.06.010

van Everdingen, R.O., 2005. Multi-Language Glossary of Permafrost and Related Ground-Ice Terms. National Snow and Ice Data Center/ World Data Center for Glaciology, Boulder, CO.

Walter, K.M., Edwards, M.E., Grosse, G., Zimov, S.A., Chapin, F.S., 2007. Thermokarst Lakes as a Source of Atmospheric CH_4 During the Last Deglaciation. Science 318, 633–636. https://doi.org/10.1126/science.1142924

Walter, K.M., Zimov, S.A., Chanton, J.P., Verbyla, D., Chapin, F.S., 2006. Methane bubbling from Siberian thaw lakes as a positive feedback to climate warming. Nature 443, 71–75. https://doi.org/10.1038/nature05040

Wetterich, S., Herzschuh, U., Meyer, H., Pestryakova, L., Plessen, B., Lopez, C.M.L., Schirrmeister, L., 2008. Evaporation effects as reflected in freshwaters and ostracod calcite from modern environments in Central and Northeast Yakutia (East Siberia, Russia). Hydrobiologia 614, 171–195. https://doi.org/10.1007/s10750-008-9505-y

Wetterich, S., Schirrmeister, L., Andreev, A.A., Pudenz, M., Plessen, B., Meyer, H., Kunitsky, V.V., 2009. Eemian and Late Glacial/Holocene palaeoenvironmental records from permafrost sequences at the Dmitry Laptev Strait (NE Siberia, Russia). Palaeogeogr. Palaeoclimatol. Palaeoecol. 279, 73–95. https://doi.org/10.1016/j.palaeo.2009.05.002

Yi, Y., Kimball, J.S., Chen, R.H., Moghaddam, M., Reichle, R.H., Mishra, U., Zona, D., Oechel, W.C., 2018. Characterizing permafrost active layer dynamics and sensitivity to landscape spatial heterogeneity in Alaska. The Cryosphere 12, 145–161. https://doi.org/10.5194/tc-12-145-2018

Zhang, T., Heginbottom, J.A., Barry, R.G., Brown, J., 2000. Further statistics on the distribution of permafrost and ground ice in the Northern Hemisphere [1]. Polar Geogr. 24, 126–131. https://doi.org/10.1080/10889370009377692

Appendix

*Table 3: **YUK15-YU-L7**: raw data for hydrological, biogeochemical and sedimentological parameters*

sample ID	mean depth [cm]	gravimetric water content [%]	magnetic susceptibility (LF) [10^{-8} m^3 kg^{-1}]	bulk density [g/cm^3]	DOC [mg/L]	TC [wt%]	TOC (wt%)	$d^{13}C$ (‰) vs. VPDB lin. korr.	dD (‰ vs. VSMOW)	$\delta^{18}O$ (‰ vs. VSMOW)	clay [vol%]	silt [vol%]	sand [vol%]	mean grain size [µm]
YUK15-YUL7 541-547 cm	544	24,88	87,46	1,41	155,1	1,92	0,891	-25,52	-	-	6,98%	72,94%	20,09%	21,69
YUK15-YUL7 562-566 cm	564	20,93	91,03	1,56	-	1,65	0,565	-24,67	-	-	7,26%	72,09%	20,65%	21,04
YUK15-YUL7 580-583 cm	581,5	28,85	73,84	1,28	-	3,30	2,726	-26,12	-	-	8,70%	75,79%	15,51%	17,52
YUK15-YUL7 622-630 cm	626	20,99	94,97	1,56	135,25	1,39	0,460	-24,20	-	-	8,23%	73,59%	18,18%	18,67
YUK15-YUL7 772-778 cm	775	18,07	134,92	-	201,3	0,84	0,416	-24,86	-	-	9,12%	77,15%	13,72%	15,75
YUK15-YUL7 1245-1270 cm	1257,5	60,79	235,42	0,52	-	0,29	< 0,10	-	-	-	2,11%	17,93%	79,96%	141,2
YUK15-YUL7 1299-1305 cm	1302	15,92	174,66	-	96,6	0,30	< 0,10	-	-134,29	-13,67	1,98%	21,47%	76,54%	131,9
YUK15-YUL7 1325-1331 cm	1328	20,16	171,11	1,59	-	1,25	0,550	-24,81	-134,40	-13,57	5,65%	62,25%	32,11%	31,34
YUK15-YUL7 1395-1400 cm	1397,5	19,16	142,25	-	163,25	1,00	< 0,10	-	-	-	6,07%	68,72%	25,21%	27,59
YUK15-YUL7 1529-1539 cm	1534	20,03	241,08	1,59	108,5	0,54	< 0,10	-	-130,52	-13,06	2,66%	30,07%	67,27%	94,15
YUK15-YUL7 1645-1653 cm	1649	22,99	118,53	1,48	152,45	1,17	0,494	-25,02	-129,02	-12,74	5,30%	65,20%	29,50%	33,72
YUK15-YUL7 1688-1696 cm	1692	19,31	106,53	-	174,65	1,24	0,533	-25,14	-	-	4,76%	71,99%	23,24%	33,46
YUK15-YUL7 1703-1711 cm	1707	20,33	100,29	1,58	186,45	1,18	0,520	-25,06	-	-	5,82%	73,41%	20,77%	28,42
YUK15-YUL7 1758-1767 cm	1762,5	23,90	156,81	1,45	-	2,76	2,130	-26,07	-	-	6,05%	77,21%	16,74%	23,51
YUK15-YUL7 1792-1800 cm	1796	18,61	91,48	-	-	1,26	0,552	-24,79	-130,41	-12,86	6,17%	74,66%	19,16%	26,34
YUK15-YUL7 1843-1855 cm	1849	20,09	94,72	1,59	207,9	1,24	0,536	-24,78	-	-	6,43%	73,18%	20,39%	26,35
YUK15-YUL7 1919-1924 cm	1921,5	21,47	71,72	1,54	242,4	1,75	0,897	-25,21	-	-	7,04%	78,99%	13,97%	21,79
YUK15-YUL7 1933-1939 cm	1936	22,88	105,16	1,48	-	2,90	1,657	-25,12	-	-	7,44%	79,76%	12,80%	18,31
YUK15-YUL7 1960-1969 cm	1964,5	20,64	129,04	1,57	220,35	1,94	0,839	-24,93	-	-	8,02%	76,60%	15,38%	19,07

*Table 4: **YUK15-YU-L15**: raw data for hydrological, biogeochemical and sedimentological parameters*

sample ID	mean depth [cm]	gravimetric water content [%]	magnetic susceptibility (low frequency) [10^{-8} m^3 kg^{-1}]	bulk density [g/cm^3]	DOC [mg/L]	TC [wt%]	TOC (wt%)	$d^{13}C$ (‰) vs. VPDB lin. korr.	dD (‰ vs. VSMOW)	$\delta^{18}O$ (‰ vs. VSMOW)	clay [vol%]	silt [vol%]	sand [vol%]	mean grain size [µm]
YUK15-YUL15 629-635 cm	632	26,47	93,61	1,36	614,5	2,72	1,904	-24,42	-	-	8,20%	77,45%	14,35%	17,55
YUK15-YUL15 638-647 cm	642,5	26,38	119,45	1,36	557,5	2,88	2,028	-24,60	-	-	9,61%	75,48%	14,91%	16,04
YUK15-YUL15 766-772 cm	769	24,28	106,05	1,43	455,4	1,95	1,120	-24,16	-	-	7,71%	72,95%	19,34%	20,75
YUK15-YUL15 1222-1236 cm	1229	13,86	207,56	-	436,7	0,40	< 0,10	-	-	-	2,32%	25,24%	72,44%	123,71
YUK15-YUL15 1263-1268 cm	1265,5	17,07	179,96	-	139,65	0,31	< 0,10	-	-188,49	-26,09	1,73%	16,17%	82,09%	161,74
YUK15-YUL15 1280-1284 cm	1282	16,00	216,09	-	96,25	0,19	< 0,10	-	-186,56	-25,82	1,67%	10,60%	87,72%	212,12
YUK15-YUL15 1291-1297 cm	1294	13,97	177,91	-	93,6	0,17	< 0,10	-	-184,20	-25,33	0,94%	7,05%	92,00%	260,47
YUK15-YUL15 1314-1319 cm	1316,5	16,15	214,17	-	133,75	0,32	< 0,10	-	-185,60	-25,81	2,24%	19,64%	78,11%	140,54
YUK15-YUL15 1332-1336	1334	16,73	223,14	-	142,4	0,40	< 0,10	-	-186,98	-25,91	2,32%	21,29%	76,38%	134,25
YUK15-YUL15 1358-1362	1360	19,05	200,85	-	147,45	0,60	< 0,10	-	-186,83	-26,18	4,82%	50,17%	45,01%	47,64
YUK15-YUL15 1375-1380	1377,5	19,68	261,68	-	223,95	0,66	< 0,10	-	-	-	-	-	-	-
YUK15-YUL15 1400-1406	1403	17,02	172,87	-	165,3	0,32	< 0,10	-	-186,56	-25,89	1,78%	14,92%	83,30%	151,68
YUK15-YUL15 1410-1415	1412,5	18,24	189,35	-	234,35	0,58	< 0,10	-	-187,03	-26,02	-	-	-	-
YUK15-YUL15 1427-1437	1432	22,15	183,78	1,51	275,8	0,74	< 0,10	-	-188,96	-26,44	3,47%	44,77%	51,75%	61,80
YUK15-YUL15 1453-1458	1455,5	16,42	177,27	-	241,15	0,40	< 0,10	-	-	-	-	-	-	-
YUK15-YUL15 1463-1468	1465,5	16,38	280,17	-	-	0,22	< 0,10	-	-186,69	-25,99	3,21%	17,98%	78,81%	118,44
YUK15-YUL15 1479-1487	1483	15,59	325,28	-	166,85	0,23	< 0,10	-	-189,17	-26,09	-	-	-	-
YUK15-YUL15 1530-1534	1532	23,63	157,73	1,46	212,3	0,71	< 0,10	-	-192,08	-26,24	3,80%	52,93%	43,26%	53,52
YUK15-YUL15 1549-1553	1551	25,49	156,43	1,39	211,1	0,80	< 0,10	-	-194,55	-26,42	-	-	-	-
YUK15-YUL15 1564-1568	1566	22,70	243,82	1,49	219,1	0,76	< 0,10	-	-195,99	-26,63	3,00%	40,73%	56,27%	67,64
YUK15-YUL15 1582-1586	1584	20,58	331,91	1,57	-	0,46	< 0,10	-	-192,49	-25,89	-	-	-	-
YUK15-YUL15 1613-1616	1614,5	22,43	199,05	1,50	373,25	0,84	< 0,10	-	-198,71	-26,93	3,38%	48,54%	48,09%	56,61
YUK15-YUL15 1625-1631	1628	23,59	187,92	1,46	-	0,92	< 0,10	-	-199,08	-26,92	-	-	-	-
YUK15-YUL15 1644-1650	1647	30,36	176,03	1,23	688	2,05	0,997	-25,63	-199,86	-26,94	5,90%	73,66%	20,44%	25,37

*Table 4.2: **YUK15-YU-L15**: raw data for hydrological, biogeochemical and sedimentological parameters*

sample ID	mean depth [cm]	gravimetric water content [%]	magnetic susceptibility (low frequency) [10^{-8} m^3 kg^{-1}]	bulk density [g/cm^3]	DOC [mg/L]	TC [wt%]	TOC (wt%)	$d^{13}C$ (‰) vs. VPDB lin. korr.	dD (‰ vs. VSMOW)	$\delta^{18}O$ (‰ vs. VSMOW)	clay [vol%]	silt [vol%]	sand [vol%]	mean grain size [µm]
YUK15-YUL15 1644-1650	1647	30,36	176,03	1,23	688	2,05	0,997	-25,63	-199,86	-26,94	5,90%	73,66%	20,44%	25,37
YUK15-YUL15 1653-1657	1655	32,14	175,33	1,18	1168,5	3,00	1,845	-25,90	-	-	-	-	-	-
YUK15-YUL15 1670-1674	1672	32,08	178,53	1,18	1331	3,56	2,449	-26,11	-204,53	-27,42	5,69%	76,31%	17,99%	24,45
YUK15-YUL15 1682-1687	1684,5	28,61	167,74	1,29	-	2,36	1,262	-25,10	-205,51	-27,60	-	-	-	-
YUK15-YUL15 1699-1702	1700,5	16,48	199,92	-	606,5	0,36	< 0,10	-	-201,63	-27,14	2,69%	26,27%	71,04%	99,42
YUK15-YUL15 1702-1705	1703,5	15,10	179,37	-	-	0,45	< 0,10	-	-201,61	-27,00	-	-	-	-
YUK15-YUL15 1725-1730	1727,5	25,66	209,38	1,38	529,5	0,95	< 0,10	-	-206,35	-27,77	3,76%	42,52%	53,72%	59,35
YUK15-YUL15 1756-1760	1758	19,46	194,45	-	484,4	0,43	< 0,10	-	-202,23	-26,48	-	-	-	-
YUK15-YUL15 1760-1764	1762	18,96	173,49	-	552	0,44	< 0,10	-	-211,23	-28,03	3,12%	23,98%	72,90%	105,99
YUK15-YUL15 1767-1777	1772	29,73	119,87	1,25	893,5	1,64	0,931	-25,74	-213,42	-28,22	-	-	-	-
YUK15-YUL15 1790-1798	1794	18,21	233,42	-	968,5	0,56	< 0,10	-	-215,09	-28,40	3,04%	25,82%	71,14%	101,71
YUK15-YUL15 1812-1816	1814	91,41	-	0,09	51,21	-	-	-	-220,53	-28,83	-	-	-	-
YUK15-YUL15 1817-1823	1820	75,89	-	0,28	138,5	-	-	-	-225,96	-29,16	-	-	-	-
YUK15-YUL15 1812-1823	1817,5	-	162,23	-	-	1,23	0,532	-	-	-	4,51%	56,72%	38,77%	42,47
YUK15-YUL15 1823-1826	1824,5	31,65	137,36	-	670,5	1,34	0,629	-25,55	-226,86	-29,19	-	-	-	-
YUK15-YUL15 1832-1836	1834	19,32	181,63	1,62	1140,5	0,66	< 0,10	-	-228,09	-29,21	3,06%	30,32%	66,63%	96,03
YUK15-YUL15 1847-1852	1849,5	20,03	203,06	-	976	0,57	< 0,10	-	-229,34	-29,39	-	-	-	-
YUK15-YUL15 1865-1873	1869	22,15	166,57	1,51	1619,5	1,09	< 0,10	-	-229,36	-29,52	4,95%	58,97%	36,07%	36,51
YUK15-YUL15 1879-1884	1881,5	26,18	179,81	1,37	1248	1,20	0,515	-25,19	-227,63	-29,47	-	-	-	-
YUK15-YUL15 1897-1902	1899,5	24,71	157,43	1,42	1275,5	1,24	0,528	-25,21	-217,87	-29,06	4,40%	54,60%	40,99%	43,62
YUK15-YUL15 1928-1935	1931,5	26,44	127,02	1,36	1132	1,40	0,618	-25,20	-230,42	-29,55	-	-	-	-
YUK15-YUL15 1955-1960	1957,5	26,24	116,69	1,36	1076	1,42	0,612	-25,21	-227,77	-29,11	4,76%	59,53%	35,70%	38,98
YUK15-YUL15 1971-1976	1973,5	33,64	123,15	1,13	716	1,43	0,618	-25,40	-227,69	-29,18	-	-	-	-
YUK15-YUL15 1989-1995	1992	52,76	108,02	0,67	447,8	2,22	1,424	-25,37	-225,02	-28,90	6,53%	76,10%	17,37%	21,62

*Table 4.3: **YUK15-YU-L15**: raw data for hydrological, biogeochemical and sedimentological parameters*

sample ID	mean depth [cm]	gravimetric water content [%]	magnetic susceptibility (low frequency) [10^{-8} m^3 kg^{-1}]	bulk density [g/cm^3]	DOC [mg/L]	TC [wt%]	TOC (wt%)	$d^{13}C$ (‰) vs. VPDB lin. korr.	dD (‰ vs. VSMOW)	$\delta^{18}O$ (‰ vs. VSMOW)	clay [vol%]	silt [vol%]	sand [vol%]	mean grain size [µm]
YUK15-YUL15 2043-2051	2047	50,95	67,35	0,71	449,9	1,13	< 0,10	-	-215,98	-28,12	-	-	-	-
YUK15-YUL15 2064-2073	2068,5	68,23	80,52	0,40	170,3	1,11	< 0,10	-	-208,34	-27,28	8,33%	75,52%	16,15%	19,19
YUK15-YUL15 2097-2103	2100	43,51	74,24	0,87	179,4	1,10	< 0,10	-	-201,24	-26,64	9,28%	78,44%	12,28%	16,24
YUK15-YUL15 2122-2126	2124	46,76	70,85	0,80	257,5	1,32	< 0,10	-	-199,48	-26,49	9,37%	80,26%	10,36%	15,82

Acknowledgement

This thesis was carried out at the Alfred Wegener Institute, Helmholtz Center for Polar and Marine Research in Potsdam. Therefore my special thanks goes to my supervisors Dr. Jens Strauss and Loeka Jongejans, who raised my interest in ongoing environmental changes in the Arctic, supported me during the writing process and were eager to transfer their knowledge and experience in this research field.

Special thanks goes to Dyke Scheidemann, who is an excellent laboratory supervisor and without whom the sedimentological labs at the AWI Potsdam would not run as smoothly as they do. Thanks to Torben Windirsch-Woiwode and Hanno Meyer for supporting me during the data analyses.
Furthermore, I want to thank all my colleagues and friends in the AWI Permafrost section for integrating me in such a friendly and open way and sharing their knowledge with me.

A very big thank you goes out to my family and friends, who always supported me during my years of study in Dresden, Augsburg and Potsdam. Thanks for your encouragement, trust, support, and interest. Last but not least, thank you Vinzenz for being so patient and understanding and having always an open ear for the smaller and bigger challenges concerning my studies.

Independence statement/ Eigenständigkeitserklärung

Eidesstattliche Erklärung zur Masterarbeit

Hiermit erkläre ich, die vorliegende Masterarbeit selbständig und lediglich unter Verwendung der angegebenen Quellen und Hilfsmittel verfasst zu haben.
Sämtliche Stellen, die wörtlich oder sinngemäß aus veröffentlichten oder noch nicht veröffentlichten Quellen entnommen wurden, sind als solche kenntlich gemacht.
Die Zeichnungen oder Abbildungen in dieser Arbeit sind von mir selbst erstellt oder mit einem entsprechenden Quellennachweis versehen worden.

Ich erkläre weiterhin, dass die vorliegende Arbeit noch nicht im Rahmen eines anderen Prüfungsverfahrens eingereicht wurde.

Potsdam,

Statutory Declaration

I hereby declare that I have authored this master thesis independently and that I have not used other than the declared sources/ material. All passages which were quoted directly or in modified form are indicated as such.

Furthermore I declare that this master thesis has not been submitted as a part of any other examination.

Potsdam,